Numeric Solution of the Non-Linear Omega Equation

by

WARREN KENNETH JONES
B.Sc., University of Minnesota, 1979

A THESIS SUBMITTED IN PARTIAL FULFILLMENT OF THE REQUIREMENTS FOR THE DEGREE OF MASTER OF SCIENCE

in the Department of Computer Science

We accept this thesis as conforming to the required standard

[redacted]
Dr. Maurice Danard

[redacted]
Dr. D. Dale Olesky

[redacted]
Dr. Frank Roberts

[redacted]
Dr. Denton E. Hewgill

[redacted]
Dr. Fausto Milinazzo

UNIVERSITY OF VICTORIA
August 1985

Supervisor: Dr. Maurice Danard

Abstract

Cloud patterns observed in satellite photos are associated with areas of upward motion. A method is described for incorporating this information into 500 mb analysis and prediction. The key lies in the solution of the omega equation:

$$-\frac{\partial\psi}{\partial y}\frac{\partial}{\partial x}(\nabla^2\psi + f) + \frac{\partial\psi}{\partial x}\frac{\partial}{\partial y}(\nabla^2\psi + f) = a\nabla^2\omega + b\omega$$

This nonlinear third order equation describes the relation between horizontal winds — represented by the stream function ψ — and the vertical velocity ω.

A stable numerical method, based on integration along characteristics, is presented for a linearized form of the problem. Computation of ψ is followed by the use of the balance equation

$$2(\psi_{xx}\psi_{yy} - \psi_{xy}^2) + f\nabla^2\psi + \nabla f \cdot \nabla\psi = g\nabla^2 z$$

to recover the 500 mb height field z. Errors in z introduced by solution of the linearized omega equation are found to be less than 10 meters in a typical case.

An algorithm for the nonlinear omega equation is discussed, involving the solution of a series of linearized problems. This iteration is found to be divergent.

Examiners:

[redacted]

Dr. Maurice Danard

[redacted]

Dr. D. Dale Olesky

[redacted]

Dr. Frank Roberts

[redacted]

Dr. Denton E. Hewgill

[redacted]

Dr. Fausto Milinazzo

Table of Contents

List of Tables

List of Figures

Figure **Page**

CHAPTER I

Introduction

1.1. Horizontal and Vertical Velocity

The study of meteorology attempts to measure and predict the motion of the earth's atmosphere. Horizontal motions, from gentle breezes of a few meters per second to gales of tens of meters per second, can be observed directly. But vertical motions, though no less important in the long term development of weather, are much smaller in magnitude. The strongest large scale updrafts and downdrafts seldom measure more than a few centimeters per second.

Accurate measurement of vertical motion must therefor be indirect. One of the most useful methods is based on the fact that vertical and horizontal motions of the atmosphere are not independent. They are related by the *omega equation*, which under several simplifying assumptions described below takes the form

$$-\frac{\partial \psi}{\partial y}\frac{\partial}{\partial x}(\nabla^2\psi + f) + \frac{\partial \psi}{\partial x}\frac{\partial}{\partial y}(\nabla^2\psi + f) = a\,\nabla^2\omega + b\,\omega \qquad (1.1)$$

Given known horizontal winds, the use of equation (1.1) to find the vertical velocity ω is well understood. In contrast, the inverse problem has received little or no attention. Starting from known values of ω, the question becomes how to determine the wind field, as represented by the stream function ψ. The numerical solution of this nonlinear third order problem is the subject of this paper.

It will be explained how a practical solution might contribute to more accurate initialization of atmospheric models. This is of interest because weather predictions can be no more accurate than the initial data on which they are based. But while meteorology provides the motivation for what follows, the emphasis will be on the mathematics, rather than the physics, of the omega equation.

1.2. Pressure Coordinates

The notation of equation (1.1) and some of the assumptions behind it need to be explained by way of preparation. To begin it should be noted that both horizontal and vertical velocities will vary with altitude. Equation (1.1) gives their relationship at a single level of the atmosphere. It might seem most natural to define this level by a constant altitude, either above sea level or above the earth's surface. But because atmospheric pressure decreases monotonically with altitude, a simple transformation allows its use as an alternative

vertical coordinate. Of the most important equations of numerical meteorology, many take their simplest form under this transformation. One of these is the omega equation. Equation (1.1) assumes a vertical axis calibrated in Pascals rather than meters, and gives the relation between horizontal and vertical velocities at a level of varying altitude but constant pressure.

The single most important level in forecasting large scale weather patterns is at 500 millibars. In terms of mass, this is approximately half way to the top of the atmosphere. The height z of this surface is typically between 5000 and 6000 meters. All the work that follows, except where specifically stated otherwise, is concerned with winds and vertical motions at the 500 mb level.

Vertical velocity, denoted by ω in equation (1.1), is also measured in pressure coordinates, i.e. Pascals/second. Note that since pressure decreases with altitude, a rising current of air will lead to a *negative* value of ω.

1.3. The Stream Function

The omega equation relates the vertical velocity ω to the horizontal winds through the stream function ψ. The wind field $\mathbf{V}$ can be represented as the sum of a rotational component $\mathbf{V}_\psi$ and a divergent component $\mathbf{V}_\chi$ (Holton, 1972), such that

$$\text{div } \mathbf{V}_\psi = \text{curl } \mathbf{V}_\chi = 0$$

While the divergent wind $\mathbf{V}_\chi$ is important in the long term balance of the

atmosphere, it is much smaller in magnitude than $\mathbf{V}_\psi$ and can be neglected with little loss of accuracy in short term forecasts. It is the rotational wind that will concern us in the work that follows. It can be computed from the stream function ψ by

$$\mathbf{V}_\psi = \mathbf{k} \times \nabla\psi \tag{1.2}$$

Equation (1.1) is based on a tangent plane coordinate system. Wind components u and v are directed along the x and y axes respectively and can be computed from equation (1.2):

$$u = -\frac{\partial\psi}{\partial y} \qquad v = \frac{\partial\psi}{\partial x} \tag{1.3}$$

It is easy to verify that $\mathbf{V}_\psi$ is non-divergent, i.e.

$$\nabla\cdot\mathbf{V}_\psi = \frac{\partial u}{\partial x} + \frac{\partial v}{\partial y} = 0$$

1.4. Vorticity

The curl of the rotational wind field is refered to as the *vorticity*. Of primary interest is the vertical component of the vorticity, given by

$$\varsigma = k\cdot(\nabla \times \mathbf{V}_\psi) = \frac{\partial v}{\partial x} - \frac{\partial u}{\partial y} \tag{1.4}$$

or, substituting wind components from (1.3)

$$\varsigma = \nabla^2\psi \tag{1.5}$$

Substitution from equations (1.3) and (1.5) leads to a more concise form of equation (1.1):

$$u \frac{\partial}{\partial x}(\varsigma + f) + v \frac{\partial}{\partial y}(\varsigma + f) = a \nabla^2 \omega + b \omega \tag{1.6}$$

or in vector form:

$$\mathbf{V}_\psi \cdot \nabla(\varsigma + f) = a \nabla^2 \omega + b \omega \tag{1.7}$$

The earth provides a rotating frame of reference for the system described by equation (1.7). The vertical component of that rotation is proportional to the coriolis parameter f, which varies with the latitude ϕ according to the formula

$$f = 2\Omega \sin\phi$$

where Ω is the angular velocity of the earth's rotation. The coriolis parameter can be regarded as the vorticity due to the earth's rotation, while ς is the inherent vorticity of the wind field, measured relative to the earth's surface. Thus the sum $\varsigma + f$ represents total or *absolute vorticity.* The expression $\mathbf{V}_\psi \cdot \nabla(\varsigma + f)$ on the left hand side of equation (1.7) is refered to as the *vorticity advection.* Freely speaking, it represents the transport of vorticity by the rotational wind. The units on both sides of (1.7) are $\sec^{-2}$, which can be interpreted as measuring a time rate of change of vorticity.

1.5. Physical Constants

On the right hand side of equation (1.7), ω represents vertical velocity in pressure coordinates as mentioned above. a and b combine several constants and have been introduced to gloss over some physical details of the problem:

$$a = -\frac{p_5\sigma}{f_0} \qquad b = \frac{2f_0}{p_5}$$

p_5 is the vertical coordinate of the surface described by equation (1.7), i.e. 5×10^4 Pascals (500 millibars). σ is a stability parameter assigned the value $2.26\times10^{-6}\ m^2\text{sec}^{-2}Pa^{-2}$. Because the right hand side of equation (1.7) is not particularly sensitive to the value of the coriolis parameter f, which varies slowly in any case, the constant $f_0 = 1.06\times10^{-4}\ \text{sec}^{-1}$ can be used here. This is an average value of f over the middle latitude region studied in the work that follows.

1.6. Simplifying Assumptions

Equation (1.7) is a simplified form of the more general omega equation derived by Haltiner and Williams (1980)

$$f_0\frac{\partial}{\partial p}[\mathbf{V}_\psi\cdot\nabla(\zeta+f)] - g\,\nabla^2(\mathbf{V}_\psi\cdot\nabla\frac{\partial z}{\partial p}) = \sigma\nabla^2\omega + {f_0}^2\frac{\partial^2\omega}{\partial p^2} \qquad (1.8)$$

In equation (1.8) p is the vertical, i.e. pressure coordinate. z is the altitude in meters above sea level of the isobaric surface, and g is the acceleration of gravity. Equation (1.8) can be reduced to equation (1.7) under four assumptions outlined by Danard (1982):

(1) Negligible contribution from the term $g\,\nabla^2(\mathbf{V}_\psi\cdot\nabla\frac{\partial z}{\partial p})$

(2) $\omega = 0$ at 1000 mb.

(3) A parabolic vertical profile for ω with a maximum at 500 mb, i.e.

$$\omega(p) = \frac{p(p_0 - p)}{p_5(p_0 - p_5)}\omega_5$$

where $p_0 = 1000$ mb, $p_5 = 500$ mb and ω_5 is the vertical velocity at 500 mb.

(4) Negligible vorticity advection at 1000 mb.

1.7. The Balance Equation

Given a known stream function ψ, equation (1.1) can be used to find the vertical velocity ω. But since ψ itself is not a directly observable quantity, a preliminary step is required. It is possible to measure the wind vector **V**, take partial derivatives of its components u and v, and then find ψ by solving the Poisson equation

$$\nabla^2\psi = \frac{\partial v}{\partial x} - \frac{\partial u}{\partial y}$$

This procedure, which effectively removes any divergent component of the observed wind, is only practical when wind measurements are abundant.

It is easier to measure the forces that give rise to observed winds than it is to measure those winds directly. At a constant altitude, winds appear to be driven by gradients of atmospheric pressure. But when we adopt p as a vertical coordinate and consider an isobaric surface, pressure gradients are by definition no longer possible. An area of high pressure appears as an elevation of the 500 mb surface, an area of low pressure as a depression. In the new coordinate sys-

tem, winds arise from these differences in elevation, or more precisely, from gradients of the geopotential $\Phi = gz$. Thus the height z of the isobaric surface becomes the primary observed variable.

The stream function ψ can then be computed from z by means of the balance equation (Bolin, 1956)

$$2(\psi_{xx} \psi_{yy} - \psi_{xy}^{\,2}) + f \nabla^2 \psi + \nabla f \cdot \nabla \psi = g \nabla^2 z \qquad (1.9)$$

Subscripts are used here to indicate partial derivatives:

$$\psi_{xx} = \frac{\partial^2 \psi}{\partial x^2} \qquad \psi_{xy} = \frac{\partial^2 \psi}{\partial x \, \partial y} \qquad \psi_{yy} = \frac{\partial^2 \psi}{\partial y^2}$$

The balance equation is so named because it gives the relation between the geopotential field and the non-divergent wind when a state of balance exists between the pressure gradient force, the coriolis force and centrifugal force. Efficient algorithms for the solution of this second order nonlinear equation in ψ are described by Arnason (1957), Paegle and Tomlinson (1974) and Iverson and Nordeng (1982). The wind field computed through the use of equation (1.9) is usually more reliable than the results of direct wind measurement.

1.8. Solving for Vertical Velocity

The use of the omega equation to determine vertical velocities is described by Clark (1962), Haltiner (1963) and Djurić (1969). (1.1) is an elliptic second order linear equation in ω. Its solution by finite difference methods presents no

special difficulties in principle. The more complete equation (1.8) introduces a third dimension through the term $\frac{\partial^2 \omega}{\partial p^2}$, but remains elliptic and linear in ω. Its solution is also well understood. Details of the solution of equation (1.1) for ω as part of experiments with the more difficult inverse problem will be described in more detail in chapter II.

The complete procedure for computing vertical velocities is as follows:

(1) Determine z (from direct observation or from a numerical model).
(2) Using z, solve the balance equation for ψ.
(3) Using ψ, solve equation (1.1) for ω.

1.9. Initializing Predictive Models

Sections 1.7 and 1.8 described the use of the 500 mb height z in computing vertical velocity. The same height field is a primary component of the initial data commonly required by numerical models of the atmosphere. If that data is inaccurate, predictions can hardly be expected to be any better. But observations are expensive and never as numerous as might be desired. This is particularly true over large expanses of the North Pacific where much of British Columbia's weather originates.

Satellite photos offer an underexploited source of supplemental information over these data sparse areas. Cloud patterns seen in those photos are the condensation associated with regions of rising air – that is to say, with negative

values of ω. The use of how satellite cloud data to compute vertical velocity fields is described by Ivanyan (1972).

Information in the form of vertical velocity data is not directly useful for the initialization of atmospheric models. Its use to supplement more traditional observations requires an effective method for solving the omega equation for ψ. Danard (1982) proposes a five step procedure to modify the height of the 500 mb surface using the extra information from satellite photos:

(1) Starting with z_0, the best 500 mb height based on conventional observations and numerical modeling, use the balance equation to find ψ_0.
(2) Compute ω_0 from ψ_0 by solving the omega equation.
(3) Use information from satellite photos to modify and correct ω_0, resulting in ω_1.
(4) Using ω_1, solve the omega equation for ψ_1.
(5) Using ψ_1, solve the balance equation for z_1.

Of the five steps in this procedure, only (4) is not well understood. This is the problem – the solution of equation (1.1) for the stream function ψ – that is treated in the following pages.

CHAPTER II

Experimental Method

2.1. Sample Data

In the absence of a comprehensive theory of nonlinear third order equations such as (1.1), methods are necessarily ad hoc and experimental. The numerical experiments described in this paper were conducted using data from the Canadian Meteorological Centre. The CMC maintains a hemispheric spectral model of the atmosphere that is regularly updated with observations from a variety of sources. Spectral coefficients from this model, though they would have been very useful, are not readily available. The CMC distributes instead values computed using those coefficients at a set of regularly spaced grid points. The most important of these grid point values to this study is z_{500}, the height in meters above sea level of the 500 mb pressure surface.

2.2. Map Projections

The area covered by the sample data, which includes the west coast from northern California to Alaska, a portion of Siberia and a large part of the North Pacific, is shown in figure (2.1). The map is a polar stereographic projection

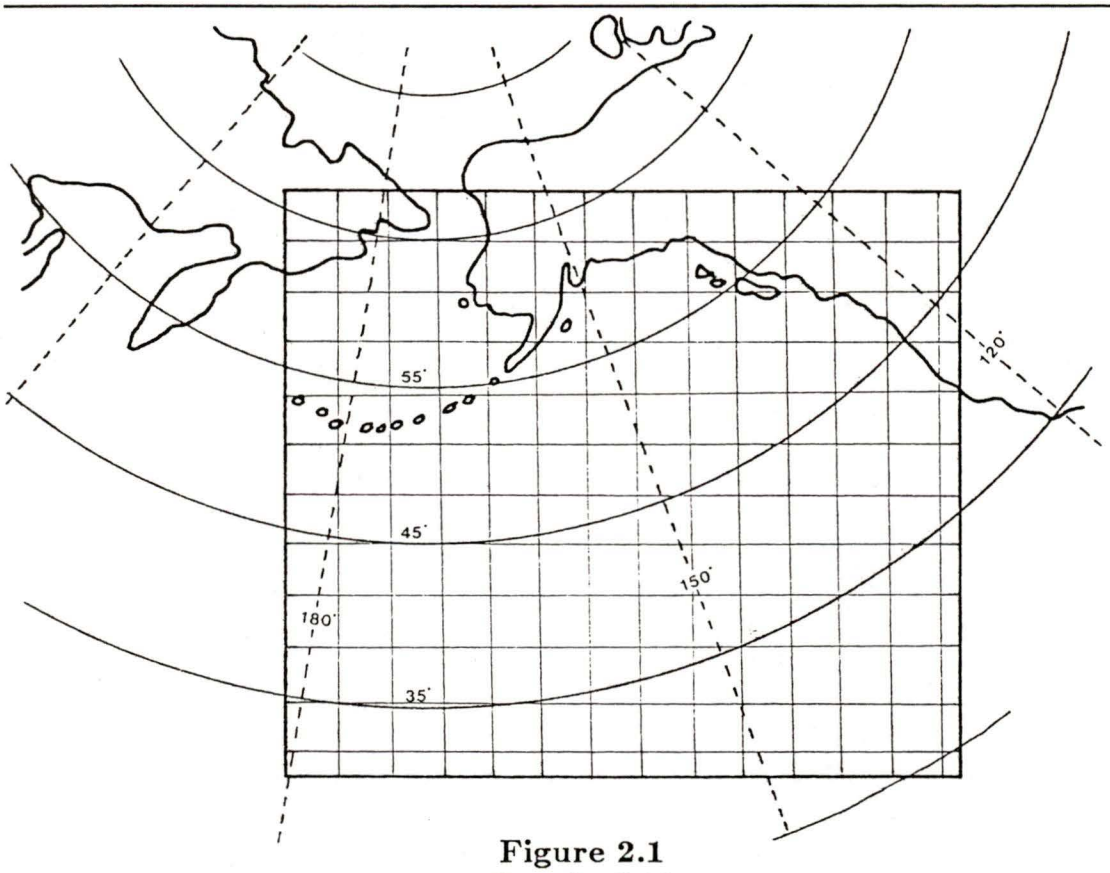

Figure 2.1
Sample Grid

with the cutting plane at 60° north latitude. The source of the projection is at the south pole, as illustrated in figure (2.2). It is clear from that diagram that areas near and south of the equator will be exaggerated, while areas in the middle and high latitudes remain relatively free of distortion.

Superimposed on the map in figure (2.1) is the 12 by 14 mesh of points at which the CMC's data is computed. The mesh is orthogonal and the points are

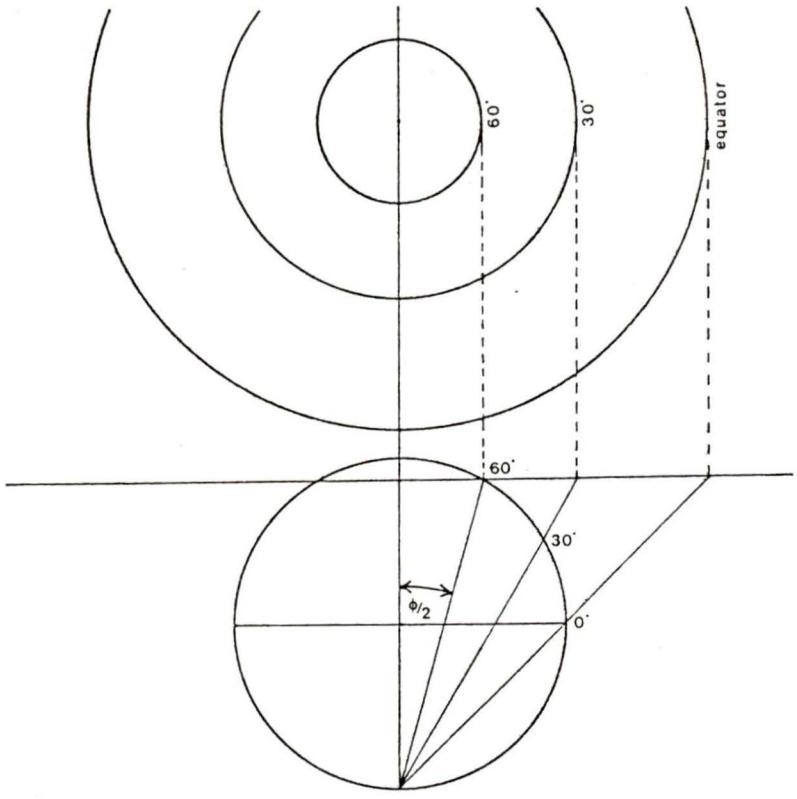

Figure 2.2
Polar Stereographic Projection

equidistant on the map projection, but the actual distance between grid points on the earth's surface varies with latitude. At 60° north the distance between grid points is $h_0 = 3.81 \times 10^5$ meters. At latitude ϕ the mesh spacing h is given by

$$h = \left(\frac{1 + \sin\phi}{1 + \sin 60^\circ}\right) h_0 \tag{2.1}$$

At all latitudes the spacing is the same along each axis in map coordinates, i.e.

$$h_x = h_y = h\,.$$

2.3. Interpolation

The 381 kilometer mesh shown in figure (2.1) does not offer particularly high resolution. In order to introduce greater detail and create a problem of more realistic computational size, interpolation was used to produce a grid with

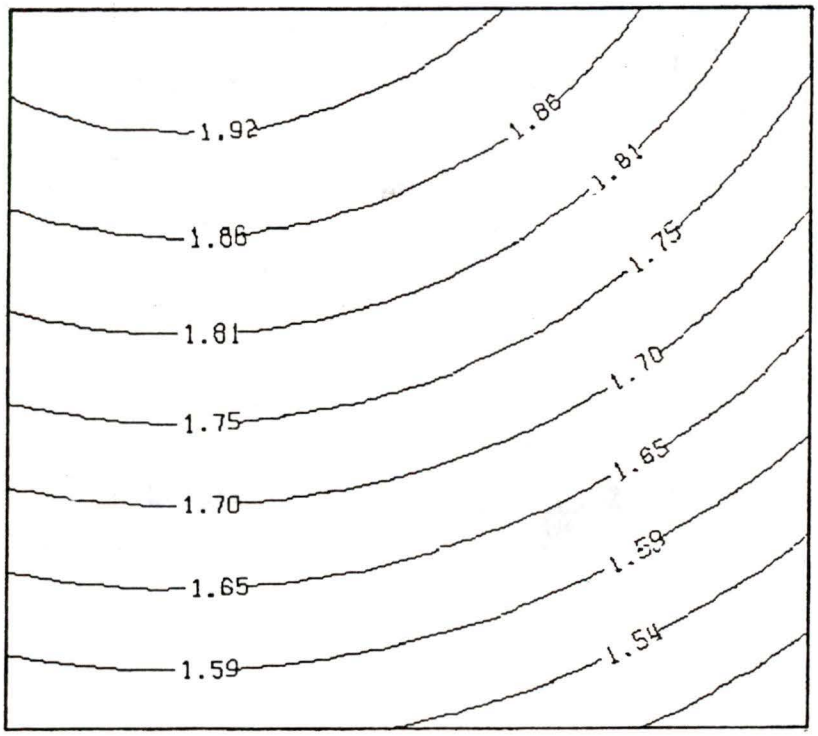

Figure 2.3
Variation of grid spacing with latitude
(10^5 meters)

half this spacing and four times as many data points. Bilinear interpolation, originally chosen as the simplest method, was found to introduce spurious short wave length components in the data that caused difficulties at a later stage. Because interpolation to a finer mesh need only be performed once, the more time consuming process of Chebyshev interpolation was justified. The data was expanded in Chebyshev polynomials along the x and y axes in turn, and the resulting coefficients were then used to compute values at intermediate points. The result is a grid measuring 28 points along the x (east-west) axis and 24 points along the y (north-south) axis. At 60° north latitude, the points of this finer mesh are 1.905×10^5 meters apart. Figure (2.3) shows the variation of mesh spacing with latitude over the sample area.

Contours of the 500 mb surface at 0000 hours GMT, 17 November 1980 are shown in figure (2.4). This data was chosen as presenting a typical problem, and provided a starting point for all the work that follows. While no algorithm can be judged a practical success without tests in a broad variety of circumstances, the results from the data of figure (2.4) will allow some useful preliminary evaluations. This data does not, however, present all difficulties that might arise in real life problems. In particular, figure (2.4) shows no closed contours. The significance of this fact will be discussed in chapter III.

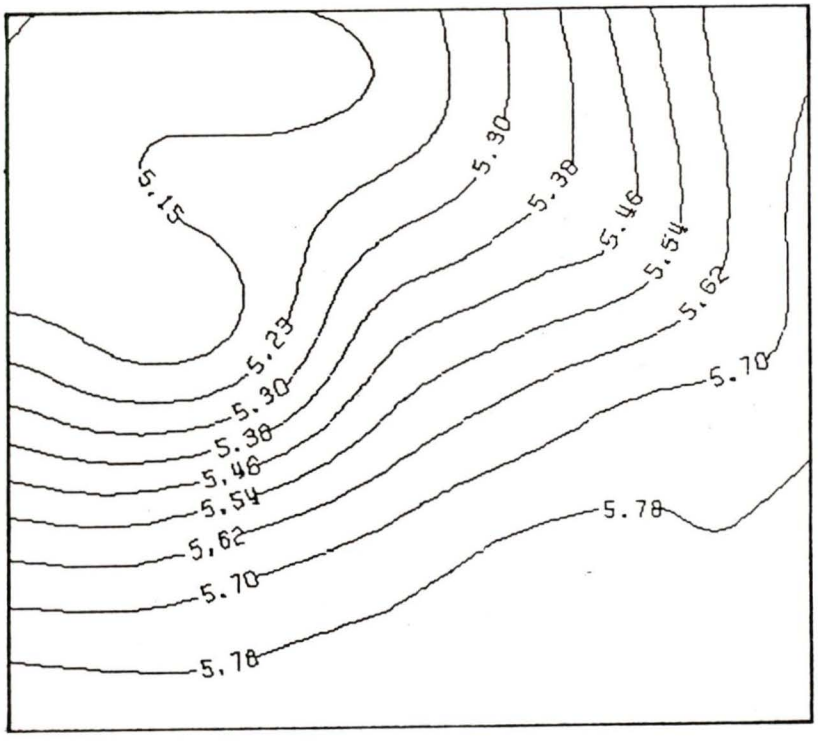

Figure 2.4
500 millibar height field
(10^3 meters)

2.4. A Five Step Procedure

Numerical experiments followed the procedure suggested by Danard (section 1.9) with only minor modifications.

(1) Compute ψ_0 from sample values of z_0, using the balance equation.
(2) Compute ω from ψ_0 using equation (1.1).

(3) The critical step: using ω from step (2), solve equation (1.1) for ψ_1.
(4) Use the balance equation to recover z_1 from ψ_1.
(5) Evaluate accuracy by comparing z_0 and z_1.

This circular protocol is illustrated in figure (2.5).

In a practical application of this procedure, the values of ω computed in step (2) would be modified on the basis of satellite cloud data. In these experiments that modification was omitted, the goal being to recover as nearly as possible the original height field. The difference between z_0 and z_1 provides a measure of the success of the critical step (3), the solution of equation (1.1) for ψ_1. The other steps present no serious difficulties, either in theory or practice. It will be shown that the errors those steps introduced in the loop illustrated in figure (2.5) were negligible.

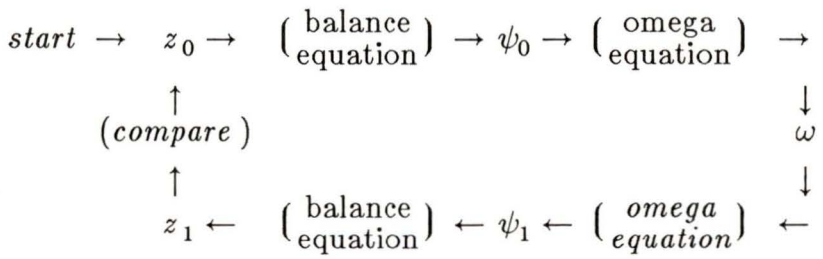

Figure 2.5
Experimental method for the omega equation

Values of z distributed by the CMC are given to the nearest meter, which reflects the uncertainties of physical measurement. A procedure leading to $\max \mid z_1 - z_0 \mid \leq 1$ meter would be judged very successful in practical terms. The 500 millibar height field illustrated in figure (2.4) has a range of about 700 meters, thus a maximum error of one meter would represent not quite three decimal places of accuracy. It will be seen in the following chapters how closely this standard was approached, and under what conditions.

2.5. Solving the Balance Equation

The experimental procedure illustrated in figure (2.5) involves two solutions of the balance equation. It is used first to compute the stream function ψ_0 from the height field z_0. A second solution – this time in the opposite direction – recovers z_1 from ψ_1.

Equation (1.9) is second order and nonlinear in ψ. While it is solved more or less routinely using methods described by Iverson, Nordeng and others, these algorithms are expensive in terms of CPU time and by no means trivial to code. This effort is justified when maximum accuracy is required, for example in CMC forecasting. The less stringent requirements of this problem allowed the use of a shortcut. The balance equation was used here only to provide a standard of accuracy in inverting the omega equation. It is difficult to judge the success of this procedure strictly by comparing ψ_0 and ψ_1. Since the stream function is

not a directly measured physical variable, it is not clear if a discrepancy between original and recovered values is significant or if it is consistent with uncertainties of observation. The balance equation was used to link stream functions ψ_0 and ψ_1 to height fields z_0 and z_1, for which a clear standard of comparison does exist. An algorithm can be judged successful in practical terms if z_0 and z_1 are everywhere in agreement to within a meter or less.[1]

For this purpose it is not required that translations between ψ and z be physically accurate to the last decimal, only that they be consistent. The equation obtained by dropping the nonlinear terms from (1.9) satisfies this requirement while being much easier to solve:

$$f\nabla^2\psi + \nabla f\cdot\nabla\psi = g\nabla^2 z \tag{2.2}$$

Equation (2.2) was solved by finite difference methods on the grid shown in figure (2.1). Second order centered difference approximations were used for the Laplacian, i.e.

$$\nabla^2\psi_0 = \frac{1}{h^2}(\psi_1+\psi_2+\psi_3+\psi_4-4\psi_0) + O(h^2) \tag{2.3}$$

where subscripts correspond to the numbering of grid points in the computational molecule illustrated in figure (2.6). Second order centered differences for first partial derivatives led to the approximation of the inner product

---

[1]An even simpler, though less accurate, translation between the stream function and the 500 mb height field can be based on the geostrophic approximation $\psi \approx \frac{g}{f}z$.

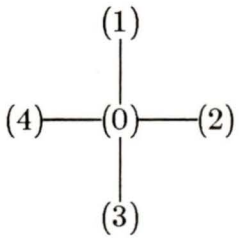

Figure 2.6
Computational molecule for $\nabla^2\psi$

$$\nabla f \cdot \nabla \psi = \frac{1}{4h^2}(f_2 - f_4)(\psi_2 - \psi_4) + \frac{1}{4h^2}(f_1 - f_3)(\psi_1 - \psi_3) + O(h^2) \tag{2.4}$$

Note that h is not a constant in equations (2.3) and (2.4), but varies with latitude according to the relation given in equation (2.1). The resulting system of difference equations, while not strictly diagonally dominant, is very nearly so, and Gauss-Seidel iteration converges rapidly to a solution.

Boundary conditions for ψ were determined from the relation given by Bolin (1956)

$$\frac{\partial \psi}{\partial s} = \frac{g}{f}\frac{\partial z}{\partial s} - \frac{1}{S}\oint \frac{g}{f}\frac{\partial z}{\partial s} ds \tag{2.5}$$

where s is distance measured counterclockwise around the boundary, and

$$S = \oint ds$$

is the total length of the boundary. This is based on the geostrophic approximation

$$\frac{\partial \psi}{\partial s} = \frac{g}{f}\frac{\partial z}{\partial s}$$

with the addition of a constant term to insure that

$$\oint \frac{d\psi}{ds} ds = 0$$

ψ was arbitrarily set equal to zero in the lower left hand (southwest) corner of the study region, and numerical integration of (2.5) proceeded around the boundary using the trapezoidal rule.

Using CMC 500 millibar heights for z_0, equation (2.2) was solved by overrelaxation for ψ_0. Values of ψ derived from the boundary relation (2.5) were used as a first approximation. Iteration was continued until successive approximations agreed everywhere to a tolerance of 1 $m^2/\text{sec.}^2$ The resulting 500 mb stream function, shown in figure (2.7), was used as the starting point for all the following experiments.

Using these values of ψ_0, the balance equation was solved again, this time to recover the height field z_1. A second order centered difference approximation was again used for $\nabla^2 z$, with boundary values of z determined from

$$\frac{\partial z}{\partial s} = \frac{f}{g}\frac{\partial \psi}{\partial s} - \frac{f}{F}\oint \frac{f}{g}\frac{\partial \psi}{\partial s} ds$$

where

---

[2]Details of this computation are found in appendix A.

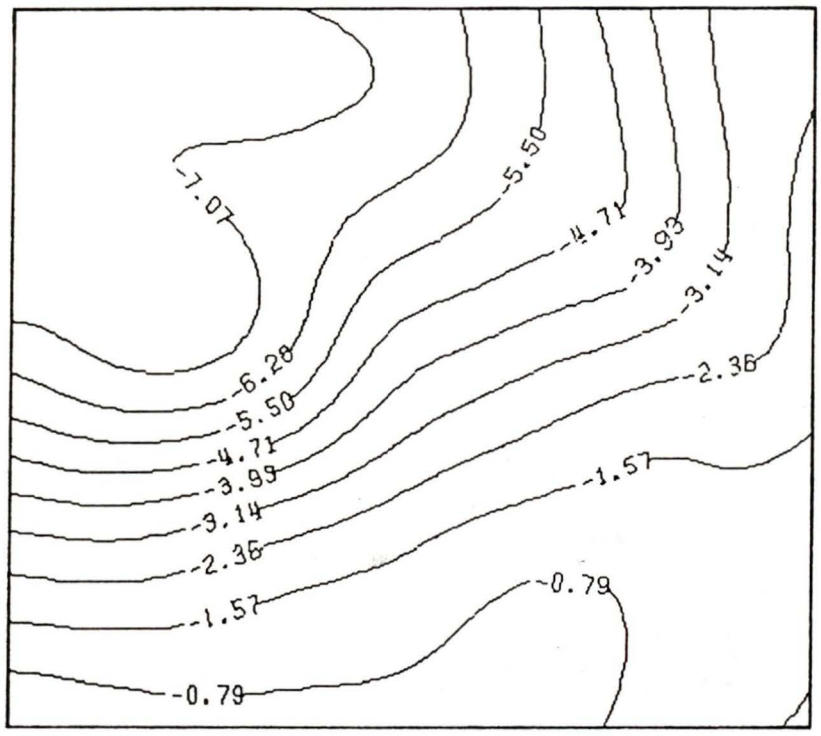

Figure 2.7
500 millibar stream function
(10^7 *meters*^{2}/sec)

$$F = \oint f ds$$

In order that subsequent steps might proceed with *complete* confidence in the accuracy of these preliminaries, iteration was continued until successive approximations agreed to 10^{-12} meters (nearly full machine precision). z_1 and z_0 were found to agree everywhere to a tolerance of less than 10^{-4} meters, a discrepancy

entirely overshadowed by uncertainties of observation.[3] From this it is safe to conclude that no significant error is introduced into the procedure outlined in section (2.4) by the solution of the balance equation in steps (1) and (4).

The 500 mb stream function ψ_0 computed in this manner is shown in figure (2.7). This is the stream function that was used in all the following experiments.

2.6. Solving for Vertical Velocity

2.6.1. Approximations for Vertical Velocity Terms

Like the solution of equation (2.2), the solution of equation (1.1) for ω is a linear second order problem that poses no special difficulties. The second order centered difference formula of equation (2.3) was again used for $\nabla^2\omega$, leading to the difference equation

$$\frac{a}{h^2}(\omega_1 + \omega_2 + \omega_3 + \omega_4 - 4\omega_0) + b\,\omega_0 = A_0$$

where subscripts refer to the computational molecule illustrated in figure (2.6). Here A_0 represents the vorticity advection term from the left side of equation (1.1), a known function of x, y and ψ. Rearranging terms gives

$$(b - \frac{4a}{h^2})\omega_0 + \frac{a}{h^2}(\omega_1 + \omega_2 + \omega_3 + \omega_4) = A_0 \qquad (2.6)$$

[3]Details of this computation are found in appendix A.

Since a and b are of opposite sign,

$$| b - \frac{4a}{h^2} | > 4 | \frac{a}{h^2} |$$

thus making the system of difference equations strictly diagonally dominant and insuring the convergence of Gauss-Seidel iteration.

2.6.2. Approximations for Vorticity Advection

There are several possible finite difference approximations for the vorticity advection term

$$A_0 = - \frac{\partial \psi}{\partial y} \frac{\partial}{\partial x}(\nabla^2 \psi + f) + \frac{\partial \psi}{\partial x} \frac{\partial}{\partial y}(\nabla^2 \psi + f)$$

Two of these deserve serious consideration. Computational molecules are illustrated in figure (2.8). For both molecules (a) and (b), the first step involves computing the vorticity $\varsigma = \nabla^2 \psi$ at grid points (1), (2), (3) and (4) using the five point centered difference approximation of equation (2.3). Approximation (a) continues with computation of first derivatives with respect to x between points (2) and (4):

$$\frac{\partial \varsigma}{\partial x} = \frac{1}{2h}(\varsigma_2 - \varsigma_4) + O(h^2), \; etc.$$

First derivatives with respect to y are computed between points 1 and 3:

$$\frac{\partial \varsigma}{\partial y} = \frac{1}{2h}(\varsigma_1 - \varsigma_3) + O(h^2), \; etc.$$

leading finally to the approximation

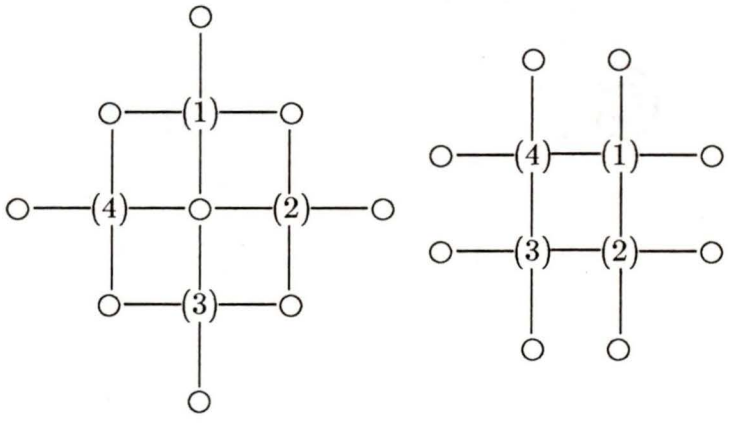

(a) (b)

Figure 2.8
Two computational molecules for vorticity advection

$$A_0 = \frac{-1}{4h^2}(\psi_1 - \psi_3)(\zeta_2 - \zeta_4 + f_2 - f_4) + \frac{1}{4h^2}(\psi_2 - \psi_4)(\zeta_1 - \zeta_3 + f_1 - f_3) + O(h^2) \tag{2.7}$$

at the central point of molecule (a).

First derivatives for molecule (b) are based on a 45° clockwise rotation of the coordinate axes. Because vorticity advection is the inner product of two vectors, this rotation leaves it unaffected. The new x-axis is parallel to the diagonal joining points (2) and (4) in (b), and the grid distance h must be multiplied by a factor of $\sqrt{2}$. We now have

$$\frac{\partial \varsigma}{\partial x} = \frac{1}{\sqrt{2}h}(\varsigma_2 - \varsigma_4) + O(h^2), \text{ etc.}$$

at the midpoint of segment $\overline{(2)(4)}$, and similarly

$$\frac{\partial \varsigma}{\partial y} = \frac{1}{\sqrt{2}h}(\varsigma_1 - \varsigma_3) + O(h^2), \text{ etc.}$$

and finally the approximation

$$\begin{aligned} A_0 = {} & \frac{-1}{2h^2}(\psi_1 - \psi_3)(\varsigma_2 - \varsigma_4 + f_2 - f_4) + \\ & \frac{1}{2h^2}(\psi_2 - \psi_4)(\varsigma_1 - \varsigma_3 + f_1 - f_3) + O(h^2) \end{aligned} \tag{2.8}$$

at the center of molecule (b). Note that although (2.7) and (2.8) appear almost identical, they are based on different numbering schemes.

The central point of molecule (a) at which vorticity advection is computed is a mesh point of the original grid. In contrast, molecule (b) gives vorticity advection on a staggered grid, offset one half step from the original in both the x and y directions. This complication is associated with several advantages. First, the step size used in (b) for computing first derivatives is $\sqrt{2}h$ rather than $2h$, resulting in a leading error term that is smaller by a factor of 2. Second, molecule (a) involves five rows and five columns of grid points, while (b) is four by four, allowing vorticity advection to be computed slightly closer to region boundaries.

These apparently minor advantages are related to a more serious concern. A differential equation can be represented by a system of difference equations

only in an approximate way. The problem is to make the correspondence as faithful as possible. As a third order equation in ψ, (1.1) can be expected to require a certain number of auxiliary conditions. But the five by five computational molecule (a) leads to a *fourth order* set of difference equations. Looking ahead to the solution of those equations for ψ, it is clear that they will require more auxiliary data than the differential equations that they are intended to represent, artificial conditions that are unrelated to the original problem. Avoiding this complication was the primary reason for chosing a finite difference approximation based on molecule (b).

2.6.3. Relaxation

Using the stream function ψ shown in figure (2.7), equation (1.1) was solved for vertical velocity by overrelaxation. Because of the choice of finite difference approximations from equations (2.6) and (2.8), the solution for ω was obtained on a 23 by 27 staggered grid. ω was set to zero on the boundary. This was chosen as an average value, and justified by the observation that values computed in the interior of the region seem relatively insensitive to perturbations near the margins.

A common problem again arose in testing for convergence. A small difference between two successive approximations may indicate an accurate solution, or it may mean only that convergence is proceeding very slowly. In

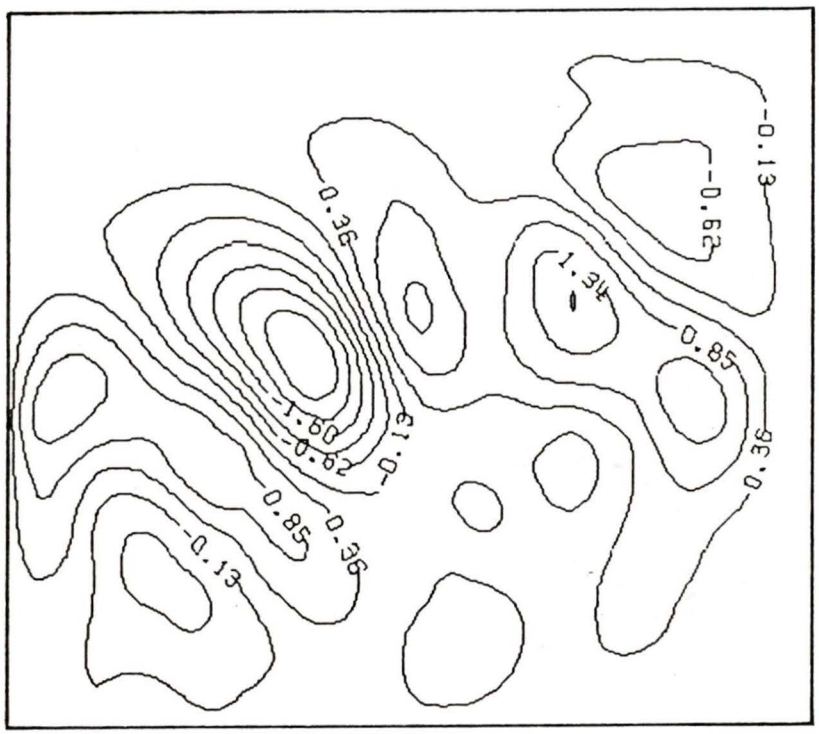

Figure 2.9
Vertical Velocity
(Pascals/sec)

this case, iteration continued until successive values of ω agreed everywhere to full machine precision (10^{-16} Pascals/sec, equivalent to about 10^{-17} meters/sec). This apparently extravagant tolerance was chosen to minimize any possible error introduced into the loop of figure (2.5) by solution for ω. A more sensible check on the accuracy of this solution by inverting equation (1.1) to recover ψ

was not possible – that being the primary problem to which this step was only a preliminary.

This procedure produced the vertical velocity field shown in figure (2.9).[4] These values of ω were used as a starting point for the next step in these experiments – solution of equation (1.1) for ψ.

[4]Details of the computation are found in appendix A.

CHAPTER III

Auxiliary Conditions

3.1. Importance of Auxiliary Conditions

The problem posed by equation (1.1) remains incomplete until appropriate auxiliary conditions have been specified. These may take the form of boundary conditions, initial conditions or some combination of the two. Choices made at this stage will lead to different methods of solution, while an incorrect choice is likely to produce nonsensical results.

Practical considerations may argue for certain types of auxiliary data. It would be convenient, for example, if the necessary values could be specified over land areas, where observations are more numerous and less costly than measurements taken over open ocean. But numerical conditions take precedence. Auxiliary conditions must be chosen to insure a well posed problem: a unique solution, with continuous dependence on the given data.

The choice of auxiliary conditions for second order linear equations is guided by a comprehensive and well developed body of theory. That theory begins by classifying all equations into three groups. For each class – elliptic,

parabolic or hyperbolic – there are appropriate methods of solution, and auxiliary conditions that will insure a well posed problem. But although certain nonlinear equations of third and higher order have been extensively studied, there is no corresponding general theory. In is possible, however, to write equation (1.1) as a system of first and second order equations, which can then be linearized in various ways. These simpler problems may throw some light on the original nonlinear equation, even if they do not lead directly to a solution.

3.2. A Linearized Problem

One simple way to write (1.1) as a pair of linked equations has already emerged:[1]

$$-\frac{\partial \psi}{\partial y}\frac{\partial}{\partial x}(\varsigma + f) + \frac{\partial \psi}{\partial x}\frac{\partial}{\partial y}(\varsigma + f) = \Omega \tag{3.1a}$$

$$\nabla^2 \psi = \varsigma \tag{3.1b}$$

For simplicity the expression $a \nabla^2 \omega + b\ \omega$, which is regarded as a known function of x and y, has been replaced by $\Omega(x, y)$. Equation (3.1a) is first order but nonlinear in both ψ and ς, while (3.1b) is second order and linear in ψ.

---

[1]In fact this will be the only alternative considered here. A less obvious possibility is discussed in appendix B.

If ψ is replaced by a known function ψ_0,[2] (3.1a) becomes a linear equation in ς:

$$-\frac{\partial \psi_0}{\partial y}\frac{\partial}{\partial x}(\varsigma + f) + \frac{\partial \psi_0}{\partial x}\frac{\partial}{\partial y}(\varsigma + f) = \Omega \tag{3.2a}$$

$$\nabla^2 \psi = \varsigma \tag{3.2b}$$

The characteristic curves along which the solution of (3.2a) propagates are the contours of ψ_0. This can be seen by writing the parametric equations for the characteristics:

$$\begin{aligned} \frac{dx}{dt} &= -\frac{\partial \psi_0}{\partial y} \\ \frac{dy}{dt} &= \frac{\partial \psi_0}{\partial x} \end{aligned} \tag{3.3}$$

Along any curve chosen from this family, ψ_0 is a function of the parameter t, and by the chain rule

$$\frac{\partial \psi_0}{\partial t} = \frac{\partial \psi_0}{\partial x}\frac{dx}{dt} + \frac{\partial \psi_0}{\partial y}\frac{dy}{dt} \tag{3.4}$$

Substitution from equations (3.3) into (3.4) gives

$$\frac{\partial \psi_0}{\partial t} = -\frac{\partial \psi_0}{\partial x}\frac{\partial \psi_0}{\partial y} + \frac{\partial \psi_0}{\partial y}\frac{\partial \psi_0}{\partial x} = 0$$

and thus $\psi_0 = \textit{constant}$ on any characteristic of (3.2a).

---

[2]Some ambiguity in the use of subscripts is unavoidable. ψ_0 is used variously to refer to:

(1) the value of ψ at a grid point labeled "0",
(2) the first function in the sequence $\psi_0, \psi_1, \psi_2 \cdots$,
(3) A known stream function as opposed to the unknown function ψ (as in this instance).

Context should provide the correct interpretation.

A first order linear equation such a (3.2a) has only a single family of characteristics, rather than the two families associated with a second order hyperbolic problem. The importance of these curves is the same, however, in both cases, and leads to similar auxiliary conditions. To be well posed, equation (3.2a) must be framed as an initial value problem, with values of ς specified along some curve Γ. If by mischance that curve coincides with a characteristic, there will be either an infinite number of solutions or (more likely) no solution. And since ς propagates along the characteristics, Γ must intersect each of these curves within the region of interest to allow a complete solution. For the sample stream function illustrated in figure (2.7), the curve made up of west and south boundaries of the region fills these requirements. Note, however, that since some streamlines intersect these boundaries at more than one point, it is possible that this could lead to an overdetermined problem. Care must be taken that inconsistent auxiliary data does not create a problem with no solution.

It must be stressed that the choice of the initial curve Γ is dependent on the shape of the stream function ψ_0. In particular, if ψ_0 includes isolated closed contours, it will not be possible for Γ to lie entirely along the boundaries of the region, as it can in this case. Dropping for a moment the assumption of a known stream function ψ_0 in equation (3.2a) and returning to the original non-

linear equation, it appears – disturbingly enough – that the placement of initial data may be intimately dependent on the very solution being sought.

Once equation (3.2a) has been solved for ς, (3.2b) can be solved for ψ. This is simply Poisson's equation, the prototype of an elliptic problem, and the required auxiliary conditions are well understood. If (3.2b) is framed as an initial value problem, the Cauchy-Kowalewski theorem guarantees the existence of an unique solution (at least if the functions involved are analytic). But in practice, this approach can produce a problem that is disastrously ill conditioned.[3] As a boundary value problem, however, Poisson's equation is well behaved. The simplest way to meet this requirement is by specifying ψ all around the perimeter. Figure (3.1) shows combined auxiliary conditions for the problem as linearized in equations (3.2a) and (3.2b).

3.3. An Alternate Linearization

It is reasonable to ask if another method of linearizing equation (1.1) might lead to different auxiliary conditions. One alternative is readily apparent. If ς is replaced by a known function ς_0, (3.1a) becomes a linear equation in ψ:

---

[3]A dramatic example is given by Hadamard (1923).

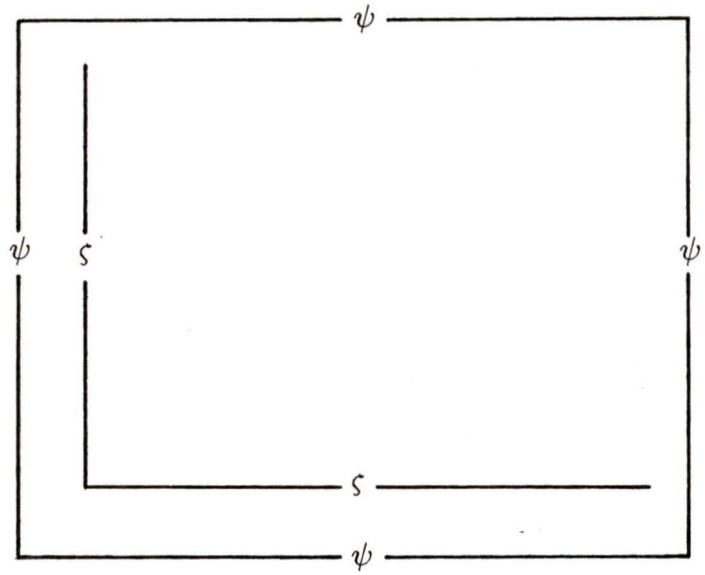

Figure 3.1
Auxiliary data for the linearized problem
Values of ψ and ς provided on the indicated contours.

$$-\frac{\partial\psi}{\partial y}\frac{\partial}{\partial x}(\varsigma_0 + f) + \frac{\partial\psi}{\partial x}\frac{\partial}{\partial y}(\varsigma_0 + f) = \Omega \tag{3.5a}$$

$$\nabla^2\psi = \varsigma \tag{3.5b}$$

There are two reasons why this alternative appears unpromising. First, it reduces the problem from third to first order. It seems unlikely that such a drastic simplification will offer much useful information about the original equa-

tion.

The second difficulty is less theoretical and more practical. The characteristics of equation (3.5a), along which the solution for ψ propagates, are the contours of $\varsigma_0 + f$ (by the same reasoning used to find the characteristics of equation 3.2a). Figure (3.2) shows the contours of $\varsigma + f$ that correspond to the

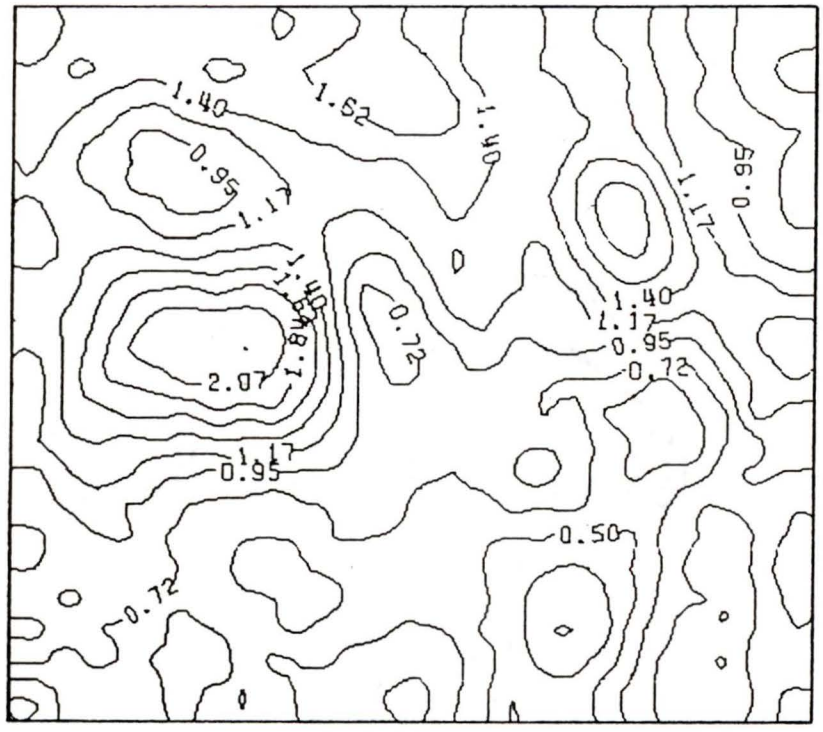

Figure 3.2
Absolute Vorticity $\varsigma + f$
(10^{-4} sec^{-1})

stream function ψ illustrated in figure (2.7). The method of solution developed in chapter IV will involve numerical integration along the characteristics, a procedure that looks reasonable for the relatively smooth and simple streamlines of ψ. In contrast, the intricate and broken contours of $\varsigma + f$ promise serious difficulties. The situation is aggravated further by the requirement that initial values of ς be specified on some curve intersecting every characteristic in the region of interest. It is clear that such a curve will have to be quite complicated, and can hardly be expected to follow region boundaries.

Behind the very different appearance of the contours in figures (2.7) and (3.2) are the two differentiations involved in computing $\varsigma = \nabla^2\psi$ from ψ. Integration is a smoothing operation, but differentiation has the opposite effect, magnifying any noise and irregularities in computing the vorticity from the stream function.

3.4. Auxiliary Conditions for the Nonlinear Problem

Some variations are possible on the auxiliary conditions illustrated in figure (3.1). Values of ψ specified on the boundary make equation (3.2b) into a Dirichlet problem. If the wind component tangent to the boundary – i.e. the normal derivative of ψ – is specified instead, the resulting Neumann problem is still well posed. Other initial curves for ς can also be chosen, within the constraints discussed above. These alternatives apply to the linearized problem of

equations (3.2a) and (3.2b). What conclusions can be drawn from this analysis about auxiliary conditions required for the nonlinear equation (1.1)?

The linearized problem is in effect a subset of the original nonlinear case, obtained through the knowledge of some extra information – specifically, the stream function ψ_0. Nothing in the nature of the problem is changed. Its solution is simply begun with half the work already done. It seems unlikely that that task would be any easier, or that conditions for the solution could be relaxed, if the extra information were not available. This admittedly informal reasoning suggests that auxiliary conditions required by the linearized equation will be necessary for the nonlinear equation as well. The question of whether those conditions will also be sufficient remains unanswered. Without the guidance of a general theory of nonlinear third order equations, it can only be resolved by the success of numerical experiments.

CHAPTER IV

The Linearized Omega Equation

4.1. An Unstable Method

This chapter will discuss the solution of the linearized system

$$-\frac{\partial \psi_0}{\partial y}\frac{\partial}{\partial x}(\varsigma + f) + \frac{\partial \psi_0}{\partial x}\frac{\partial}{\partial y}(\varsigma + f) = \Omega \tag{4.1a}$$

$$\nabla^2 \psi = \varsigma \tag{4.1b}$$

The results will provide the basis for an algorithm for the nonlinear omega equation, which will be presented in chapter V. A description of a straightforward but unsuccessful approach to the linearized problem will help to make clear some of its difficulties while pointing the way toward a better method.

The experiments described in this chapter used values of ψ_0 taken from the 500 millibar stream function illustrated in figure (2.7). This is the stream function that was used to compute the vertical velocity that enters into the expression $\Omega = a \nabla^2 \omega + b \omega$ on the right hand side of equation (3.2a), and which should be finally recovered by a successful solution of equations (3.2a) and (3.2b). It may seem paradoxical that the chosen ψ_0 is actually identical to the

exact solution ψ. Thus the solution for ς that is pursued with such labor in the following pages could be trivially obtained (though only in this contrived test case) through the identity $\nabla^2\psi_0 = \varsigma$. This relation between ψ_0 and ς, though it can hardly be expected in practice, does not diminish the usefulness of the experiment. It does provide a convenient standard for checking the accuracy of computed values of ς.

The computational molecule for vorticity advection from figure (2.8) is shown again in figure (4.1), this time as part of the larger finite difference grid. Initial values of ς are specified along the curve Γ that lies just within the west and south boundaries of the region. (Because these values of ς were computed from ψ_0 using a five point centered difference formula, Γ cannot lie directly on the boundary.) Thus ς is known at points (2), (3) and (4) of the molecule in the southwest corner of the grid. The value $\Omega_0 = a\nabla^2\omega + b\omega$ can be computed (using the second order centered difference approximation of equation 2.6) at the central point of that molecule. According to equation (4.1a), this must be equal to the vorticity advection, which can be approximated according to equation (2.8). We thus have:

$$\begin{aligned} &\frac{-1}{2h^2}(\psi_1 - \psi_3)(\varsigma_2 - \varsigma_4 + f_2 - f_4) + \\ &\frac{1}{2h^2}(\psi_2 - \psi_4)(\varsigma_1 - \varsigma_3 + f_1 - f_3) = \Omega_0 \end{aligned} \tag{4.2}$$

Equation (4.2) can then be solved for the unknown vorticity at point (1):

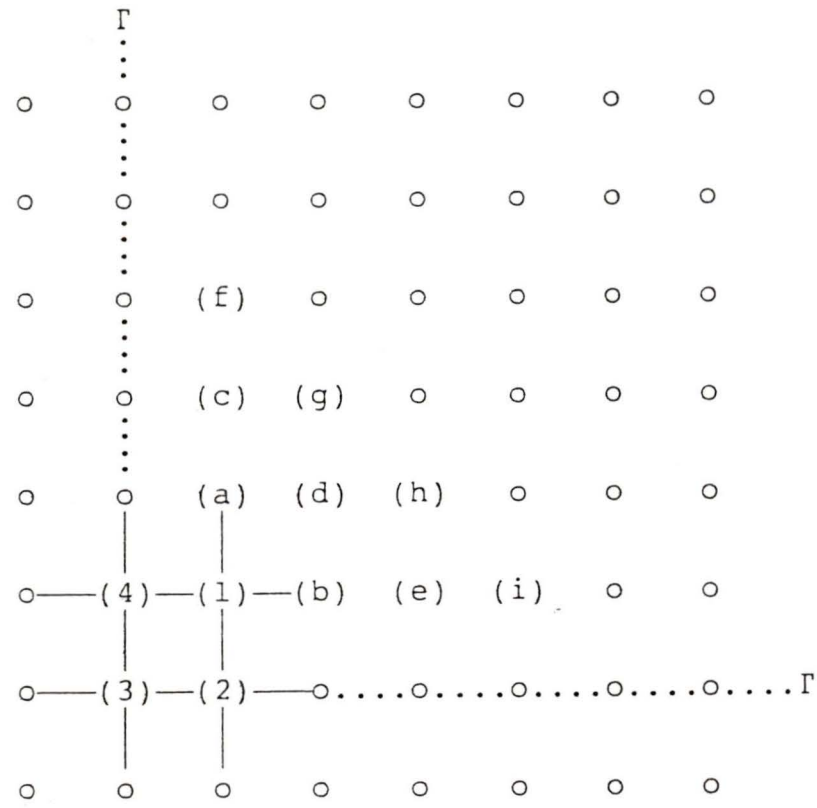

Figure 4.1
Progress of the solution for ς

$$\varsigma_1 = \varsigma_3 + f_3 - f_1 + \frac{2h^2\Omega_0 + (\psi_1-\psi_3)(\varsigma_2-\varsigma_4+f_2-f_4)}{(\psi_2-\psi_4)} \tag{4.3}$$

With this computation the solution for ς advances one step diagonally across the grid. It now becomes possible to compute ς in the same way at points (a) and (b), taking the solution forward a second step. A third step advances to points (c), (d) and (e). As this procedure is continued the solution marches

across the grid from southwest to northeast.

This method involves only the simplest algebra. If implemented without roundoff, it would certainly lead to perfect recovery of original values of ς. In practice, however, the method is subject to serious computational instability. Evidence of this instability can be seen in figure (4.2), which shows the original vorticity $\varsigma_0 = \nabla^2\psi_0$ side by side with contours of ς recovered by means of equation (4.1a) and the method described above. It can be seen that there is

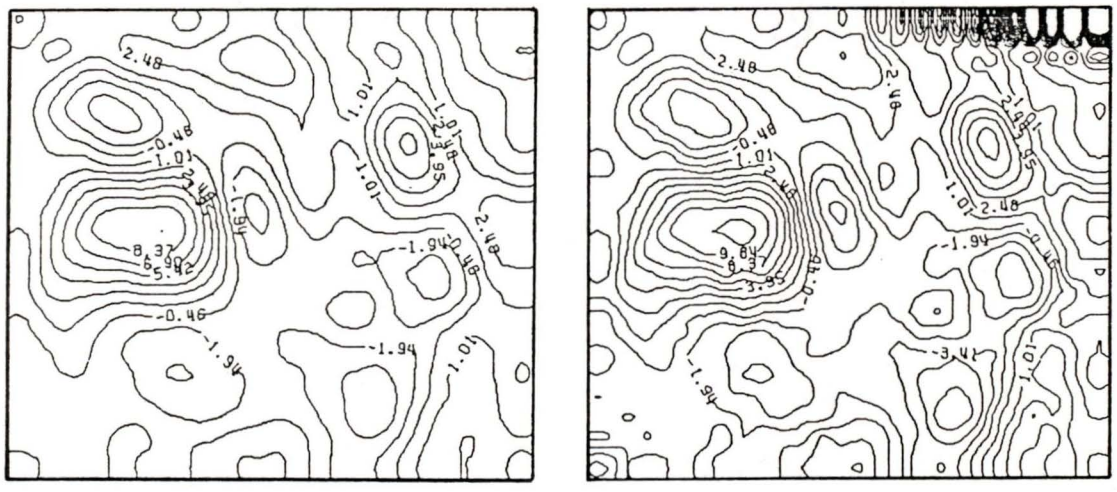

(a)
Original vorticity $\varsigma_0 = \nabla^2\psi_0$

(b)
Vorticity ς recovered by unstable solution of equation (4.1a)

Figure 4.2
ς_0 and ς (unstable method)

reasonably close agreement between these fields in the southwest corner of the region, but that the solution in (4.2b) becomes progressively contaminated with short wave length noise as it marches across the grid. A maximum error in ς of 5.5×10^{-4} sec^{-1} occurs in the northeast corner.

Since vorticity can go to zero, relative errors can be misleading, but the coriolis parameter provides a useful standard of comparison. In the following pages, errors in the computed value of ς will often be expressed as a percentage of the average value $f_0 = 1.06\times10^{-4}$ sec^{-1}. The maximum error for the method described above is 519% of f_0. Vorticity measurements differing by less than one percent of f are generally considered to be in close agreement.

A more useful comparison is made possible by solving the Poisson equation (4.1b) for the stream function ψ, and then using the balance equation to obtain the corresponding height field z. The contours of z can be compared with the original 500 millibar height field z_0 in figure (4.3). The difference between the two fields reaches a maximum of 140 meters, again in the NE corner of the region. As the cause of this instability is explained, it will be seen that only some good fortune in the shape of the stream function ψ_0 prevented it from being much more serious.

Re-examining equation (4.3) reveals the source of the problem. If $\psi_2 = \psi_4$, the denominator of the rightmost term vanishes, and solution for ς_1

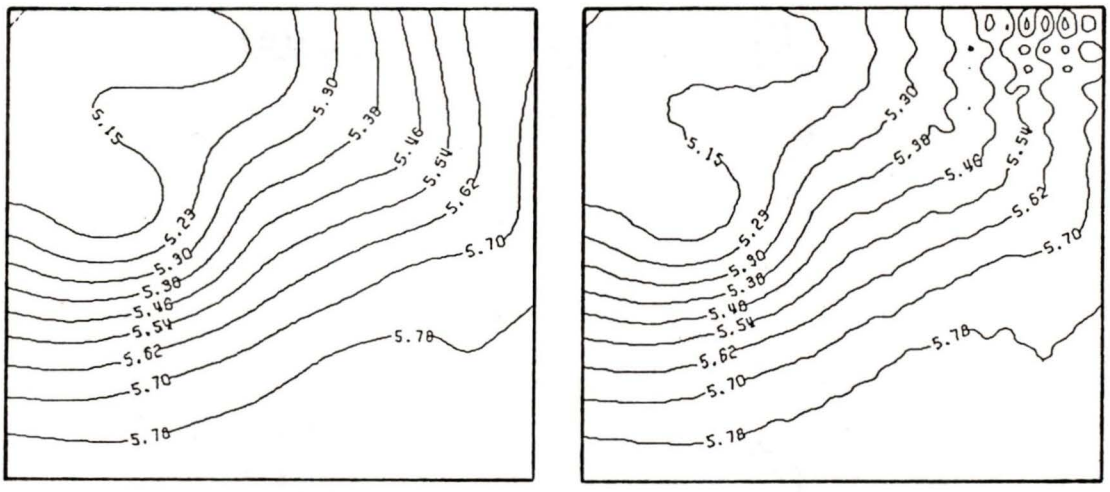

(a)
Original 500 mb height z_0

(b)
z recovered through unstable solution of equations (4.1)

Figure 4.3
z_0 and z (unstable method)

becomes impossible. This result should not be unexpected. For if $\psi_2 = \psi_4$, it means that both points lie on the same contour of ψ – that is, on the same characteristic curve of equation (4.1a). This characteristic is a barrier (because the normal derivative of ς becomes undefined), blocking extension of the solution from point (3) to point (1).

Although the quantity $\psi_2 - \psi_4$ may never completely vanish, there are still difficulties in practice when that difference becomes very small. If $\psi_2 \approx \psi_4$

there will be serious subtractive cancellation in the denominator with attendant loss of significance. If ς is not to become very large, there will have to be subtractive cancellation in the numerator as well. The resulting round off errors tend to grow exponentially, as seen in figure (4.2b).

4.2. The Courant-Friedrichs-Levy Condition

This type of computational instability was first described by Courant, Friedrichs and Levy in connection with the advection equation

$$\frac{\partial F}{\partial t} + c\frac{\partial F}{\partial x} = 0 \tag{4.4}$$

which represents the propagation of a one dimensional wave motion F with a phase velocity c. If equation (4.4) is approximated using second order centered differences on a grid with spacing Δx and Δt, it is possible to show (Haltiner and Williams, 1980) that the necessary condition for computational stability is

$$| c\frac{\Delta t}{\Delta x} | \leq 1 \tag{4.5}$$

Commonly refered to as the Courant-Friedrichs-Levy or CFL condition, (4.5) can be interpreted to mean that the time step Δt must be smaller than the interval necessary for a signal to travel the distance Δx between two adjacent grid points.

With some minor rearrangement and the substitution

$$u_0 = -\frac{\partial \psi_0}{\partial y} \qquad v_0 = \frac{\partial \psi_0}{\partial x}$$

equation (4.1a) takes a form comparable to the advection equation:

$$\frac{\partial \varsigma}{\partial y} + \left(\frac{u_0}{v_0}\right) \frac{\partial \varsigma}{\partial x} = \xi \tag{4.6}$$

where

$$\xi = \frac{\Omega_0}{v_0} - \left(\frac{u_0}{v_0}\right) \frac{\partial f}{\partial x} - \frac{\partial f}{\partial y}$$

In equation (4.6) the y coordinate plays a role analogous to t in equation (4.4). The solution for ς develops, not with time, but as we move from the SW to the NE corner of the grid (since the y axis has been chosen to lie along that diagonal). The fact that (4.6) is not homogeneous does not turn out to be particularly important. More significantly, the ratio $\frac{u_0}{v_0}$, which corresponds to the phase velocity c in (4.4), is not constant. This implies that the computational stability of the finite difference solution will vary from point to point. Since grid distances h_x and h_y (corresponding to Δx and Δt) are everywhere equal, the stability condition for (4.6) becomes simply:

$$\left| \frac{u_0}{v_0} \right| \leq 1 \tag{4.7}$$

Shaded areas in figure (4.4) show where this condition is violated by the sample values of ψ_0. Significance will be progressively lost as the solution marches through these regions.

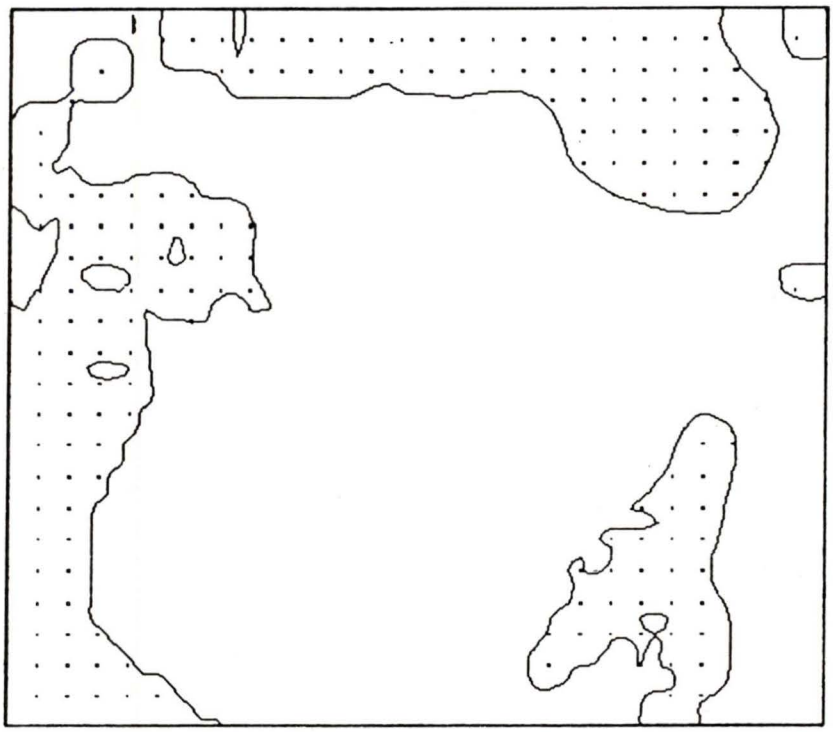

Figure 4.4
Areas of instability

Condition (4.7) can be generalized by interpreting v_0 as the wind component *parallel to the advance of the numeric solution.* The ratio $\frac{u_0}{v_0}$ then appears as the tangent of the angle between the wind vector **V** and the direction of the march of computation. Another way of stating condition (4.7) is to say that this angle must be 45° or less. This condition is intuitively reasonable.

If equation (4.1a) describes the redistribution of vorticity by the rotational wind, it is not surprising that a numerical solution for ς should be required to follow the flow of that wind. In this light it becomes clear that the instability revealed in figure (4.2b) was no worse because the computed solution, in progressing from SW to NE, did generally follow the contours of ψ_0 and the direction of the wind field.

The results are much different if initial data for ς is specified on the south and east boundaries of the region, with computation of the numeric solution from SE to NW – that is, at right angles to the previous direction of march. Solution in this manner cuts across the characteristic curves of equation (4.1a) – i.e. the contours of ψ_0 – at what is often close to a 90° angle. The shaded regions in figure (4.4) then become the only areas of stability. This leads to rapid and catastrophic breakdown, with computed values of ς in error by more than 10^{29} sec^{-1}.

4.3. Integration Along Characteristics

While the solution illustrated in figure (4.2b) is reasonably accurate over most of the grid, it is not hard to imagine a much less tractable stream function ψ_0 – one presenting large areas of instability when attacked from any given direction. Since any generally stable method can depart no more that 45° from the direction of the wind field, the best choice appears to be integrating directly

along the contours of ψ_0. This decision simplifies the problem in some respects, but also introduces some major complications.

The primary advantage in integrating along the contours of ψ_0 is that it transforms equation (4.1a) from a partial to an ordinary differential equation. In section (3.2) it was shown how those contours can be described by the parametric equations

$$\begin{aligned} \frac{dx}{dt} &= -\frac{\partial \psi_0}{\partial y} \\ \frac{dy}{dt} &= \frac{\partial \psi_0}{\partial x} \end{aligned} \tag{4.8}$$

It is convenient to replace the parameter t in equations (4.8) by the curvilinear distance s. We have

$$\frac{ds}{dt} = \sqrt{\left(\frac{dx}{dt}\right)^2 + \left(\frac{dy}{dt}\right)^2} = |\mathbf{V}_0|$$

and applying the chain rule to (4.8) results in the parametric equations

$$\begin{aligned} \frac{dx}{ds} &= -\frac{1}{|\mathbf{V}_0|}\frac{\partial \psi_0}{\partial y} \\ \frac{dy}{ds} &= \frac{1}{|\mathbf{V}_0|}\frac{\partial \psi_0}{\partial x} \end{aligned} \tag{4.9}$$

Again by the chain rule,

$$\frac{d\zeta}{ds} = \frac{\partial \zeta}{\partial x}\frac{dx}{ds} + \frac{\partial \zeta}{\partial y}\frac{dy}{ds}$$

Substituting from equation (4.9):

$$\frac{d\zeta}{ds} = \frac{1}{|\mathbf{V}_0|}\left(-\frac{\partial\psi_0}{\partial y}\frac{\partial\zeta}{\partial x} + \frac{\partial\psi_0}{\partial x}\frac{\partial\zeta}{\partial y}\right) \tag{4.10}$$

Rearranging equation (4.1a) gives

$$-\frac{\partial\psi_0}{\partial y}\frac{\partial\zeta}{\partial x} + \frac{\partial\psi_0}{\partial x}\frac{\partial\zeta}{\partial y} = \Omega - \mathbf{V}_0\cdot\nabla f$$

which on substitution into (4.10) results in an ordinary differential equation for ζ:

$$\frac{d\zeta}{ds} = \frac{1}{|\mathbf{V}_0|}(\Omega - \mathbf{V}_0\cdot\nabla f) \tag{4.11}$$

where the right hand side is a known function of x and y.

Thus ζ can be computed by simply integrating equation (4.11) along the contours of ψ_0. This is complicated in practice by the fact that any given contour will only by a remote chance pass directly through one of the nodes of the finite difference grid. Thus interpolation is necessary: both in tracing the contours of ψ_0 and in supplying values of the integrand on the right hand side of equation (4.11).

Bilinear interpolation was chosen as the simplest scheme for a first attempt at this problem. Within a single square of the grid illustrated in figure (4.5), the interpolated value of the stream function at the point (x, y) is given by

$$\psi = (1-x)(1-y)\psi_1 + (1-x)y\,\psi_2 + xy\,\psi_3 + x(1-y)\psi_4 \tag{4.12}$$

Here local coordinates x and y measure the distance, as a fraction of one grid interval, from an origin at point ψ_1. It follows from equation (4.12) that an

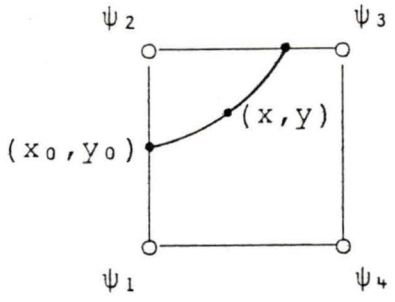

Figure 4.5
Bilinear interpolation

interpolated contour of ψ is a section of a hyperbola. This curve can be expressed in the parametric form

$$\begin{aligned} x &= ae^{t} + b \\ y &= ce^{-t} + d \end{aligned} \tag{4.13}$$

where

$$\begin{aligned} b &= (\psi_2-\psi_1)/(\psi_1-\psi_2+\psi_3-\psi_4) \\ d &= (\psi_4-\psi_1)/(\psi_1-\psi_2+\psi_3-\psi_4) \end{aligned}$$

If $t = 0$ at the point (x_0,y_0) where this contour intersects the boundary of the square, we have

$$a = x_0 - b\,, \qquad c = y_0 - d$$

This system of piecewise continuous functions provides the simplest method for reliably tracing the contours of ψ_0. But interpolation of the stream

function, which is relatively smooth and well behaved, is less troublesome than the interpolation required to provide values of the integrand on the right hand side of equation (4.11). The difficulties are apparent from a glance at the contours of $\frac{d\varsigma}{ds}$ in figure (4.6). Close examination reveals that most of the terms

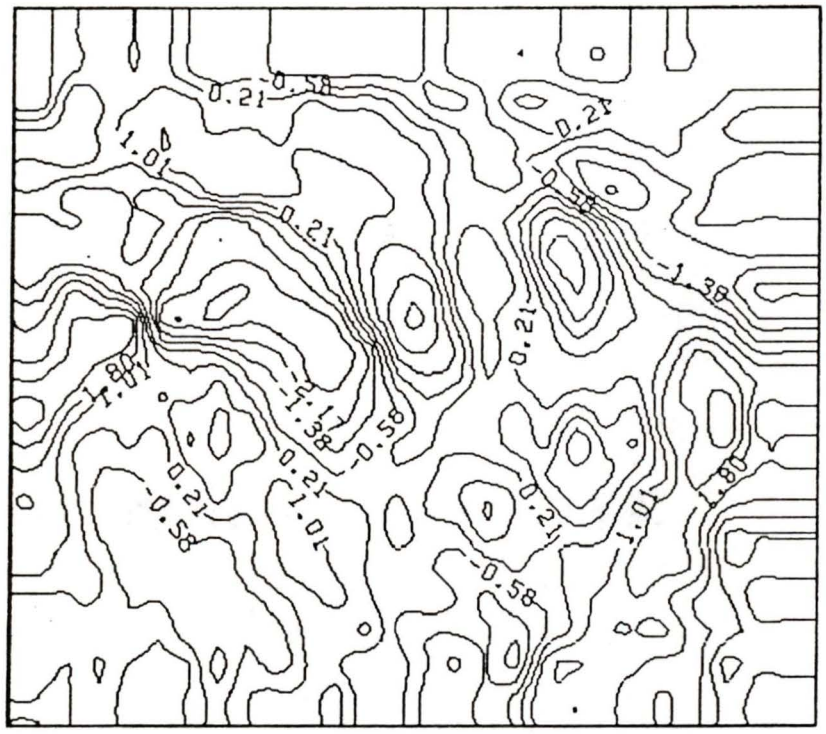

Figure 4.6

The integrand $\frac{d\varsigma}{ds}$

$(10^{-5}\ \text{sec}^{-1}\ meters^{-1})$

that contribute to this function are well behaved, and that $\nabla^2\omega$ is the primary source of irregularity. As noted in section 3.3 (in connection with the vorticity $\varsigma = \nabla^2\psi$), two differentiations serve to amplify any noise originally present in ω. Bilinear interpolation was chosen as the simplest method for a first attempt to supply values of $\frac{d\varsigma}{ds}$ along the contours of ψ_0. More elaborate methods will be discussed in section 4.7.2.

Each grid point lying on the curve Γ in figure (4.1) is associated with a known value of ς, and marks the start of a contour of ψ_0. Numerical integration proceeded along each of those characteristic curves in turn. A succession of points is generated by increases Δt of the parameter t in equations (4.13). The curvilinear distance s is related to t by

$$\frac{ds}{dt} = \sqrt{\left(\frac{dx}{dt}\right)^2 + \left(\frac{dy}{dt}\right)^2} = \sqrt{(x-b)^2 + (y-d)^2}$$

and thus

$$\Delta s \approx \Delta t \sqrt{(x-b)^2 + (y-d)^2} \tag{4.14}$$

By using (4.14), Δt can be chosen to maintain an approximately constant value of Δs. But keeping the steps exactly equal in size would be more difficult (and probably not worth the trouble). The resulting small variations of Δs mean that any integration scheme involving more than two points (say Simpson's rule) will be greatly complicated. As a result, the trapezoidal rule approxima-

tion

$$\varsigma_{n+1} = \varsigma_n + \frac{1}{2}\left[\left(\frac{d\varsigma}{ds}\right)_n + \left(\frac{d\varsigma}{ds}\right)_{n+1}\right]\Delta s$$

was used in a first attempt to generate values of ς along the characteristics.

4.4. Comparison to Original Values of ς

The procedure just described results in values of ς at a set of points irregularly distributed along the contours of integration. Only by an unlikely chance will any of these points coincide with a mesh point of the original finite difference grid. This makes it difficult to compare newly computed values of ς with the original vorticity $\varsigma_0 = \nabla^2\psi_0$, since ψ_0 and ς_0 are known only at grid points. The best that can be done is to obtain values of ς_0 at intermediate points along the contours of integration by interpolation from points on the grid. This was done using bilinear interpolation, making it possible to estimate errors in the computed values of ς. Table (4.1) shows a gradual decrease in the error in ς as the step size of integration is reduced from 1.50 to 0.10 grid intervals. The maximum error of 14.9% of f_0 obtained with a step size of 0.10 grid intervals compares quite favorably with the results of the unstable method described in section 4.1. More important, errors grow at a slow and relatively constant pace as integration proceeds along a characteristic. Figure (4.7) shows the relation of the error in ς to curvilinear distance along a characteristic. (The

Δs	points	$\lvert\varsigma - \varsigma_0\rvert$ off grid as percent of f_0		
		max	mean	rms
1.50	778	17.5	5.1	6.3
1.40	783	17.5	5.1	6.3
1.30	800	17.5	5.0	6.2
1.20	826	17.4	5.1	6.2
1.10	902	17.3	5.0	6.2
1.00	1109	17.1	5.0	6.1
0.90	1264	15.7	4.6	5.7
0.80	1301	15.3	4.5	5.5
0.70	1337	15.2	4.3	5.3
0.60	1405	16.0	4.2	5.1
0.50	1759	15.0	4.2	5.2
0.40	1988	15.0	4.1	5.1
0.30	2578	15.0	4.0	5.0
0.20	3693	14.9	4.0	5.0
0.10	6890	14.9	4.0	4.9

Table 4.1
Errors in ς along contours of integration

larger errors are the average of a small number of points, since the sample data provided many short contours but very few longer that 30 grid intervals.)

4.5. Interpolation of ς Back to Grid Points

While this improvement in accuracy is satisfying, the values of ς scattered along contours of integration are of little use in the next stage of the problem. If the Poisson equation $\nabla^2\psi = \varsigma$ is to be solved by finite difference methods

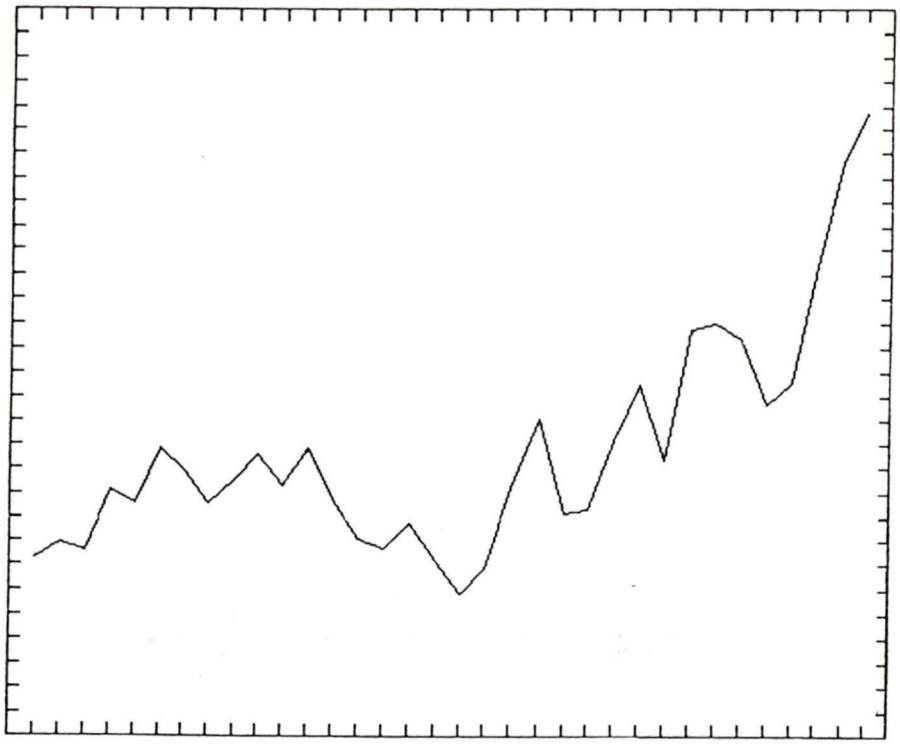

Figure 4.7
Error in ς as a function of contour length

for the stream function ψ, values of ς computed in this first stage must somehow be transferred back to the a regularly spaced grid. This was accomplished using interpolation software developed by Dr. John D. Taylor for the oceanography division of Energy, Mines and Resources Canada.[1] The EMR

[1]This interpolation routine is part of a very useful package that produced all the contour maps included in this paper. Mr. Ian Crane and Dr. T. Murty also deserve credit.

software employs a combination of two dimensional Laplace and spline interpolation. The mathematical basis for these methods is outlined by Lancaster and Salkauskas, and by Briggs (1974).

Laplace interpolation is based on the condition that $\nabla^2\zeta = 0$ at every mesh point. The resulting surface "tends to have rather sharp peaks and dips at the data points, somewhat like a trampoline with poles pushed up into it. There is no chance of spurious peaks appearing in regions devoid of data." (Taylor, Richards and Halstead, 1971)

Spline interpolation minimizes the integral

$$C(\zeta) = \int\int (\nabla^2\zeta)^2 dxdy$$

which is closely related to the total curvature of the surface. Briggs (1974) demonstrates that the solution of this variational problem corresponds to the biharmonic equation

$$\frac{\partial^4\zeta}{\partial x^4} + \frac{\partial^4\zeta}{\partial x^2\partial y^2} + \frac{\partial^4\zeta}{\partial y^4} = \nabla^4\zeta = 0 \qquad (4.15)$$

The surface produced by solution of equation of (4.15) passes smoothly through the specified points, but may have spurious peaks and steep extrapolations in areas of sparse data.

The method employed by the EMR contouring software is based on a finite difference solution of the equation

$$\nabla^2\varsigma + \kappa\nabla^4\varsigma = 0$$

For $\kappa = 0$ this results in pure Laplace interpolation, while spline interpolation predominates as $\kappa \to \infty$. The value of κ producing optimum results can be experimentally determined.

The values of ς produced by interpolation back onto grid points can be directly compared with original values of ς_0. The results can be seen in table (4.2). Comparison of table (4.2) with table (4.1) reveals that some accuracy is lost in the interpolation process, but this does not appear to be a major problem. Contours of ς_0 and ς are shown in figure (4.8). Since no increase in accuracy was obtained with a step size of integration Δs less than 0.30 grid intervals, this value was used in the following experiments.

Δs	$\lvert\varsigma - \varsigma_0\rvert$ on grid as percent of f_0		
	max	mean	rms
0.50	25.8	4.8	6.6
0.40	25.2	4.7	6.6
0.30	25.2	4.7	6.6
0.20	25.2	4.7	6.6
0.10	25.3	4.7	6.6

Table 4.2
Errors in ς after interpolation to grid points

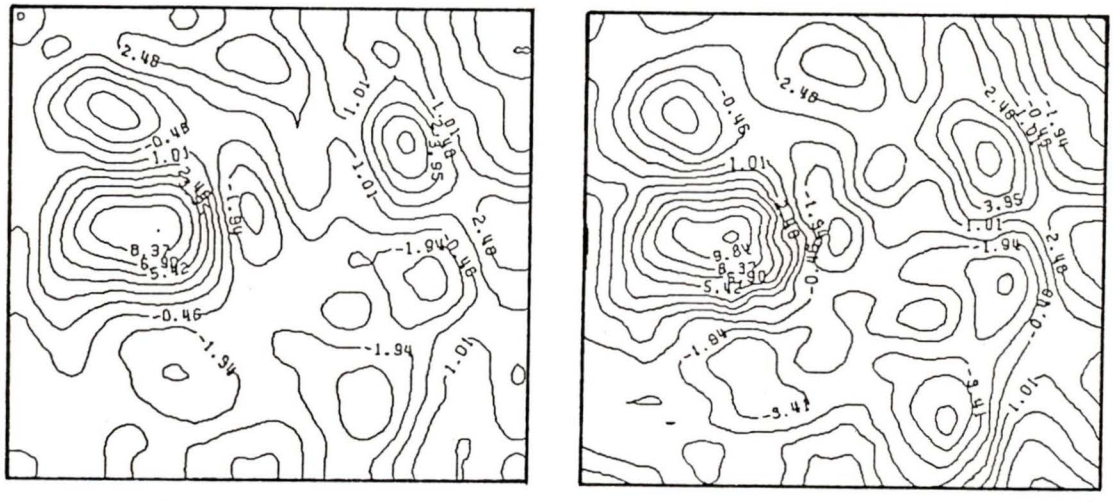

(a)
Original vorticity $\varsigma_0 = \nabla^2 \psi_0$

(b)
ς recovered by integration along contours

Figure 4.8
ς_0 and ς (stable method)

The entries in table (4.2) were computed using $\kappa = 10^6$ in the interpolation procedure described above. Table (4.3) shows corresponding errors for other values of κ (with a constant $\Delta s = 0.30$). The differences are not large, but indicate that the best results are obtained when spline interpolation is dominant. $\kappa = 10^6$ was used in all the following experiments.

4.6. Recovering the 500 mb Height Z

How significant are maximum errors in the computed value of ς amounting to approximately 25% of f_0? More meaningful comparisons are possible after completing the next two stages of the problem. Using the interpolated grid point values for vorticity, it is now possible to solve $\nabla^2\psi = \varsigma$ for the stream function ψ. Boundary values come from the original stream function ψ_0. Finally a value of the 500 mb height z corresponding to ψ can be recovered through the balance equation, as discussed in section 2.5. Figure (4.9) shows close agreement between the contours of this recovered height field and the ori-

κ	$\lvert\varsigma - \varsigma_0\rvert$ on grid as percent of f_0		
	max	mean	rms
10^{-6}	29.1	5.3	7.6
10^{-4}	29.1	5.3	7.6
10^{-2}	28.9	5.3	7.6
10^{0}	27.5	4.9	7.0
10^{2}	25.3	4.7	6.6
10^{4}	25.2	4.7	6.6
10^{6}	25.2	4.7	6.6

Table 4.3
Effect of the parameter κ on errors in ς

ginal 500 mb heights z_0. More detailed comparisons can be made in table (4.4). The maximum error in z of slightly over 15 meters falls short of the goal (errors under one meter) but is still a useful result. The mean absolute and RMS errors in z approach the level of uncertainty in physical measurements.

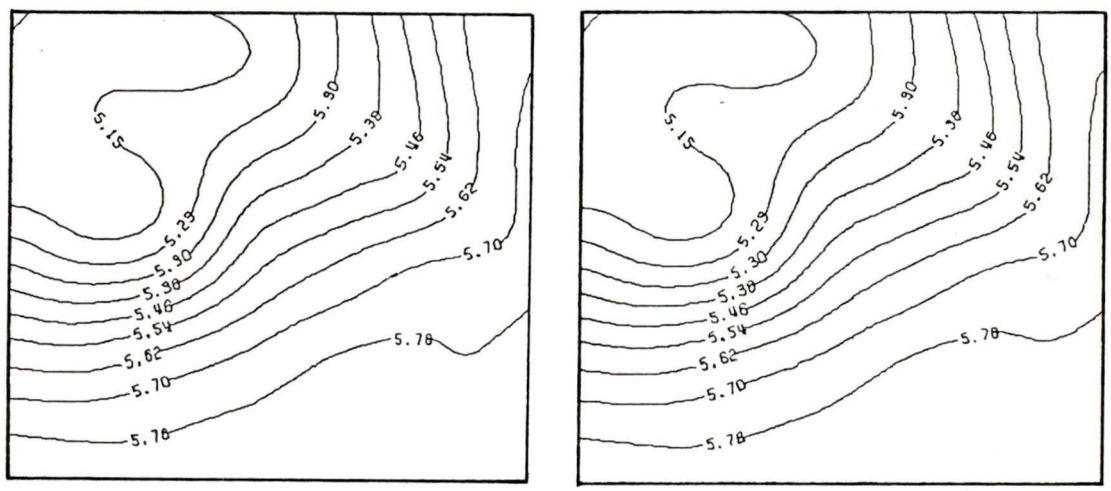

(a)
Original 500 mb height z_0

(b)
500 mb height z recovered by integration along contours

Figure 4.9
z_0 and z (stable method)

Δs	$\lvert z - z_0 \rvert$ (meters)		
	max	mean	rms
0.50	16.8	2.6	3.8
0.40	15.2	2.3	3.5
0.30	15.2	2.3	3.5
0.20	15.3	2.3	3.6
0.10	15.7	2.4	3.6

Table 4.4
Errors in recovered 500 mb height

4.7. Alternative Methods

The process of integration along characteristic curves of equation (4.1a) that led to the results seen in table (4.3) involves several rather crude approximations. More elaborate alternatives are available for:

(1) Computing the integrand $\frac{d\zeta}{ds}$

(2) Interpolating $\frac{d\zeta}{ds}$ at intermediate points along contours

(3) Numerical integration along contours

(4) Tracing contours

Some of these alternatives involve considerable expense in terms of machine computation, but increases in accuracy were found to be marginal at best. Contrary to expectation, most of the possibilities discussed below result in poorer performance.

4.7.1. Computing the Integrand $\frac{d\zeta}{ds}$

Accurate values of the integrand $\frac{d\zeta}{ds}$ are essential to a satisfactory solution of equation (4.1a). A glance at the irregular contours of figure (4.6) suggests that this function should be computed very carefully. As already noted in section 4.3, most of this irregularity can be traced to the term $\nabla^2\omega$. The Laplacian was initially computed using the second order centered difference formula of equation (2.3). A fourth order approximation for the Laplacian:

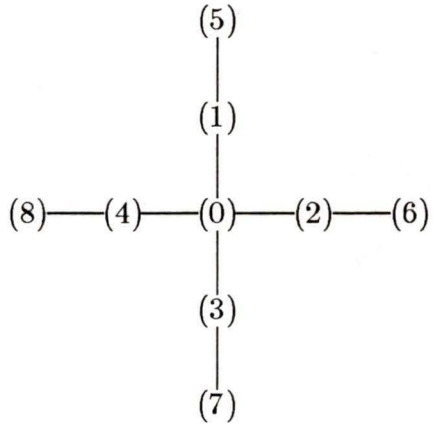

Figure 4.10
9 point computational molecule for $\nabla^2\omega$

$$\nabla^2\omega = \frac{4}{3h^2}(\omega_1+\omega_2+\omega_3+\omega_4-4\omega_0) - \frac{1}{3(2h)^2}(\omega_5+\omega_6+\omega_7+\omega_8-4\omega_0) + O(h^4) \tag{4.16}$$

is associated with the nine point computational molecule illustrated in figure (4.10). Equation (4.16) is derived from (2.3) by Richardson extrapolation. Continuing this process leads to a 13 point sixth order formula and a 17 point eighth order formula.

The results obtained by using these higher order approximations in computing $\nabla^2\omega$ and $\frac{d\varsigma}{ds}$ are shown in table (4.5). The nine and thirteen point formulas led to small improvements in accuracy of the recovered values of z (with the maximum error reduced to less than 12 meters), but errors in ς both on and off the grid are actually somewhat larger. Corresponding mean absolute and

approximation	order	max $\lvert\varsigma - \varsigma_0\rvert$ as percent of f_0		max $\lvert z - z_0 \rvert$ (meters)
		off grid	on grid	
5 point	2nd	15.0	25.2	15.2
9 point	4th	20.2	30.6	12.5
13 point	6th	23.0	30.5	11.7
17 point	8th	38.7	41.2	46.4

Table 4.5
Results from alternative approximations of $\nabla^2\omega$

RMS errors in z (not shown) are also slightly increased.

Another paradoxical observation is that the higher order approximations for the Laplacian do not correspond to the methods originally used to compute ω (see section 2.6). If the slight decreases in max $| z - z_0 |$ seen in table (4.5) are actually meaningful, it would be reasonable to expect even better performance when the vertical velocity is computed from a nine or thirteen point molecule. In fact, when these experiments are repeated with the new values of ω, errors are greatly increased. This anomalous behavior suggests that the small decreases of max $| z - z_0 |$ in table (4.5) are not significant.

4.7.2. Interpolating $\frac{d\zeta}{ds}$

Interpolation of the integrand $\frac{d\zeta}{ds}$ to intermediate points along the contours of integration is another important but troublesome part of the solution of equation (4.1a). The results discussed above were obtained using bilinear interpolation, initially chosen for its simplicity. Alternative methods include bicubic and spline interpolation.

Bicubic interpolation is based on a 4 by 4 array of grid points. The four function values in row i uniquely determine the cubic polynomial

$$\frac{d\zeta}{ds}(x, y_i) = a_i x^3 + b_i x^2 + c_i x + d$$

In the same way, coefficients a_1, a_2, a_3 and a_4 from each row determine the polynomial

$$a(y) = \hat{a}_3 y^3 + \hat{a}_2 y^2 + \hat{a}_1 y + \hat{a}_0$$

Coefficients b, c and d can be expanded along the y axis in the same manner. The interpolated value at some intermediate point (x, y) is then given by

$$\frac{d\zeta}{ds}(x, y) = a(y)x^3 + b(y)x^2 + c(y)x + d$$

Spline interpolation leads to a similar set of cubic polynomials in x and y, but coefficients are computed globally rather than locally. The value of $\frac{d\zeta}{ds}$ at any intermediate point is influenced by values at every grid point (though this influence decreases rapidly with distance). Piecewise cubic polynomials are determined to produce a continuous surface, with continuous first and second partial derivative in both x and y. Algorithms for interpolation with bicubic splines are discussed by Birkhoff (1969) and by Ahlberg et. al. (1967).

The effect of these alternative methods – both of which involve intensive machine computation – can be seen in table (4.6). Errors in the computed values of ζ are actually increased, slightly for bicubic interpolation and by almost a factor of ten for spline interpolation. It's possible to guess at an explanation of these disappointing results. Bilinear interpolation is based on function values at four nearby grid points, bicubic interpolation involves sixteen points

interpolation of $\frac{d\varsigma}{ds}$	$\lvert\varsigma - \varsigma_0\rvert$ off grid as percent of f_0		
	max	mean	rms
bilinear	15.0	4.0	5.0
bicubic	22.5	5.3	7.4
spline	126.6	19.3	26.1

Table 4.6

Effect of bicubic and spline interpolation of $\frac{d\varsigma}{ds}$

and spline interpolation involves the entire grid. But as discontinuity increases, correlation of function values at nearby points is lost. $\frac{d\varsigma}{ds}$ displays such violent local fluctuations (as can be seen from figure 4.6) that it is apparently unreliable to base interpolation on values at any but the closest grid points.

4.7.3. A Higher Order Integration Formula

The trapezoidal rule approximation

$$\int_{s_0}^{s_1} f(s)ds = \frac{1}{2}[f(s_0) + f(s_1)]h + O(h^3)$$

where $h = s_1 - s_0$ was initially used to integrate $\frac{d\varsigma}{ds}$ along the characteristics of equation (4.1a). Variations in the step size h complicate higher order

integration formulae involving more than two points. A generalization of Simpson's rule for unequal step size[2] is given by

$$\int_{s_0}^{s_2} f(s)ds = Af(s_0) + Bf(s_1) + Cf(s_2) + O((h_0+h_1)^5) \qquad (4.17)$$

where

$$h_0 = s_1 - s_0$$

$$h_1 = s_2 - s_1$$

$$A = \frac{(2h_0^3 + 3h_1h_0^2 - h_1^3)}{6h_0(h_0+h_1)}$$

$$B = \frac{(h_0+h_1)^3}{6h_0h_1}$$

$$C = \frac{(2h_1^3 + 3h_0h_1^2 - h_0^3)}{6h_1(h_0+h_1)}$$

Table (4.7) shows that use of this fifth order formula does slightly reduce the error in computed values of z, to a maximum of 10 meters. As might be expected, the best performance is obtained with a step size larger than the optimum for the trapezoid rule (about 0.7 as opposed to 0.3 grid intervals). This tends to offset the additional computation required by equation (4.17). More experience is needed to determine whether the small apparent increase in accuracy is really significant.

---

[2]MACSYMA, a LISP based symbolic manipulation system developed at MIT (©1976, 1983) was very useful in deriving this and similar formulae.

Δs	max $\lvert\varsigma - \varsigma_0\rvert$ as percent of f_0		max $\lvert z - z_0\rvert$ (meters)		
	off grid	on grid	max	mean	rms
1.20	16.7	26.1	34.3	9.9	13.6
1.10	16.9	26.2	33.3	9.7	13.2
1.00	15.7	25.3	26.4	8.3	11.0
0.90	15.2	24.5	20.1	6.0	8.0
0.80	15.1	25.2	14.3	3.9	5.2
0.70	15.1	24.4	10.0	2.4	3.3
0.60	15.0	25.2	14.6	2.4	3.5
0.50	15.0	26.0	17.4	2.6	3.9
0.40	15.0	25.4	15.5	2.3	3.5
0.30	14.9	25.1	15.1	2.3	3.5
0.20	14.9	25.4	15.6	2.4	3.6
0.10	14.9	25.3	15.7	2.4	3.6

Table 4.1
Contour integration using generalized Simpson's rule

4.1.1. Tracing the Contours of ψ_0

The use of bilinear interpolation in tracing the contours of ψ_0 leads to approximation of those curves by piecewise hyperbolas. This is not a particularly smooth approximation – the first derivative is discontinuous everywhere it crosses one of the vertical or horizontal lines of the mesh. It is tempting to try to fit a spline through the points that lie directly on the mesh lines. The resulting curve is certainly smoother, but it is unclear whether this will result in more

accurate integration. More work needs to be done with this method, but preliminary experiments were not encouraging.

CHAPTER V

The Nonlinear Problem

5.1. An Algorithm for the Nonlinear Problem

The stream function ψ_0 that enters into the linearized equation (4.1) may be a first guess at the solution of the nonlinear problem. It seems reasonable to hope that the solution (which will now be refered to as ψ_1) will be a better approximation. This naturally suggests an algorithm for the nonlinear omega equation, which proceeds as follows:

(1) Begin with a first approximation ψ_0 to the solution of equation (1.1). In a practical application of the method, this might be the original stream function from ground based observations, unmodified by satellite cloud data.

(2) Using known values of ψ_0, solve the first order linear equation

$$-\frac{\partial \psi_0}{\partial y}\frac{\partial}{\partial x}(\varsigma_1 + f) + \frac{\partial \psi_0}{\partial x}\frac{\partial}{\partial y}(\varsigma_1 + f) = a\,\nabla^2\omega + b\,\omega$$

for ς_1.

(3) Using ς_1 from step (2), solve the Poisson equation

$$\nabla^2\psi_1 = \varsigma_1$$

for ψ_1.

(4) Compare the new approximation ψ_1 with the original estimate ψ_0. If

$$\max\ |\psi_1 - \psi_0| < \textit{tolerance}$$

accept ψ_1 as the solution of equation (1.1). Otherwise let $\psi_0 = \psi_1$ and repeat from step (2).

This iteration, illustrated in figure (5.1), results in a sequence of functions ψ_0, ψ_1, ψ_2, $\psi_3 \cdots$. If the sequence converges, it will clearly be to the solution of the nonlinear equation (1.1).

5.2. Divergence of the Iteration

If this method is to be of any practical value, it must converge for any first guess ψ_0 reasonably close to the true solution ψ. We wish to find some $\epsilon > 0$ such that convergence is insured for all ψ_0, $\max \mid \psi - \psi_0 \mid < \epsilon$. The radius of convergence ϵ may be large or small – the nature of the problem gives no obvious clues. ϵ must be experimentally determined by gradually increasing the difference between ψ and ψ_0. The minimum necessary condition is that the iteration not diverge when $\epsilon = 0$, that is, for $\psi_0 = \psi$.

The critical first test of the algorithm thus involves using the known exact solution as an initial guess. This experiment results in rapid divergence after

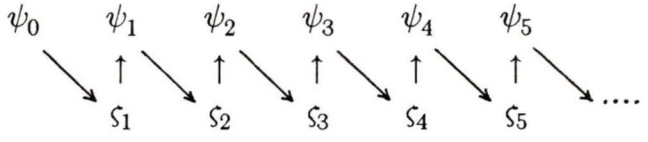

Figure 5.1
Iteration for nonlinear problem

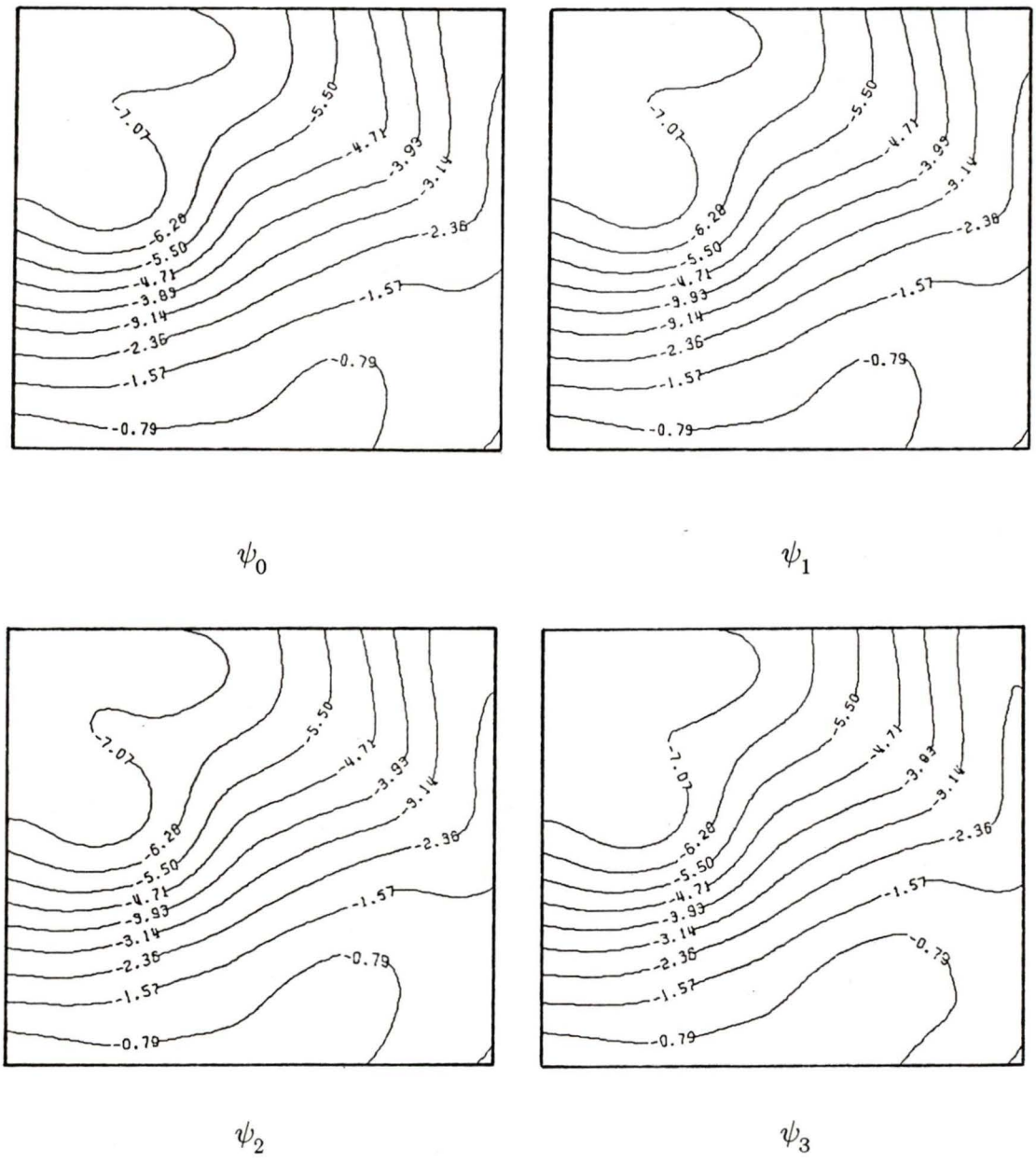

Figure 5.2
Nonlinear iteration (steps 0-3)

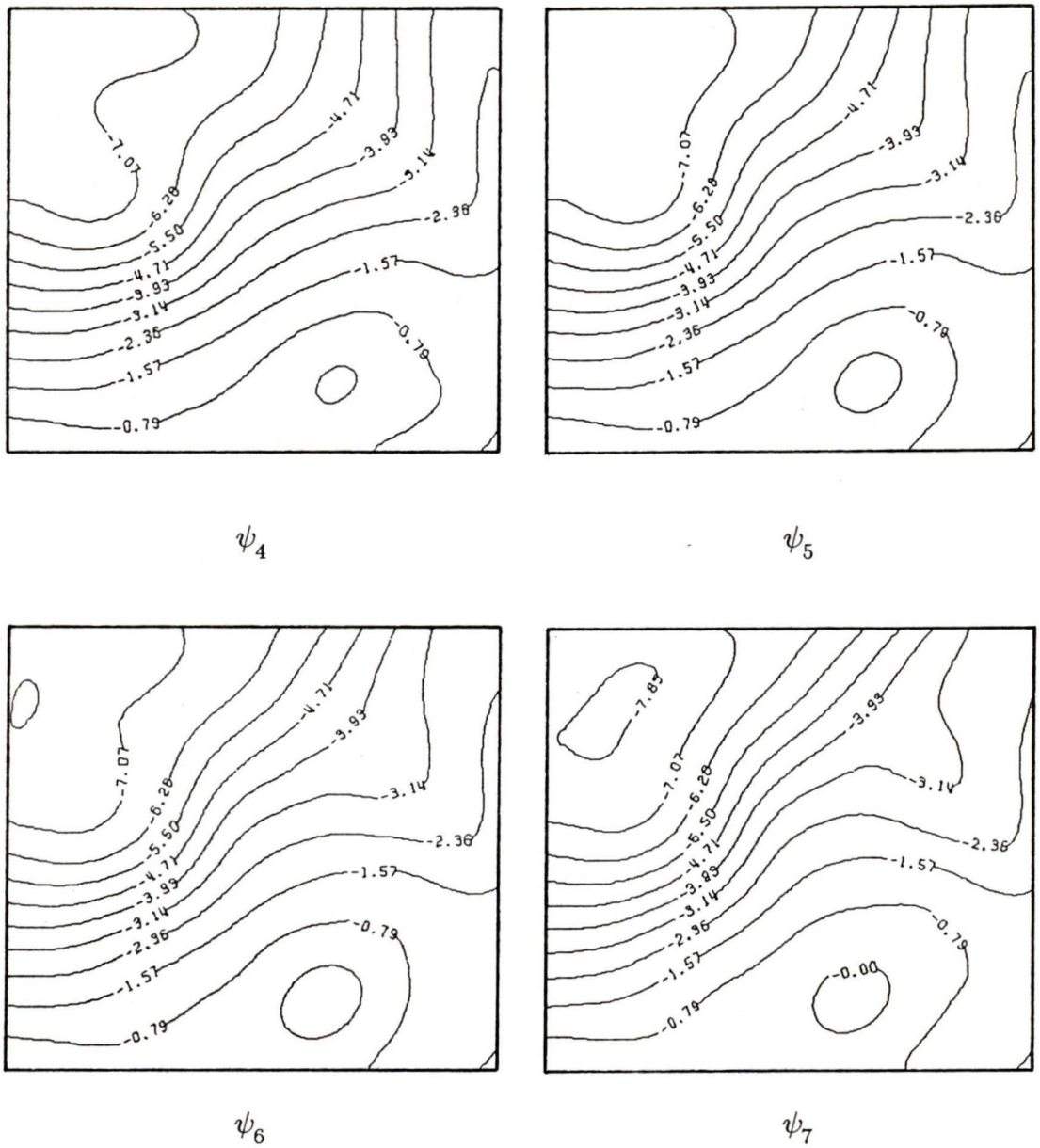

Figure 5.3
Nonlinear iteration (steps 4-7)

only eight iterations, as shown in table (5.1), and in figures (5.2) and (5.3). A point of no return is passed with the development of closed contours in step (4) (figure 5.3). The area inside those contours, which can be seen to grow in steps (5) through (7), is effectively isolated from the influence of boundary data.

Underrelaxation can sometimes be used to obtain convergence from an otherwise divergent algorithm. Letting

$$\Delta\psi_n = \psi_{n+1} - \psi_n$$

we define a new sequence ψ_1' , ψ_2' , ψ_3' $\cdots$ by

$$\psi'_{n+1} = \psi'_n + \lambda\Delta\psi_n$$

iteration (n)	max $\lvert\zeta_n-\zeta_0\rvert$ as percent of f_0	max $\lvert\psi_n-\psi_0\rvert$ (10^6 $m^2 sec^{-1}$)	max $\lvert z_n-z_0\rvert$ (meters)
0	0.0	0.00	0.0
1	25.5	1.13	15.2
2	36.8	3.03	24.5
3	61.3	4.78	40.5
4	60.4	6.93	61.8
5	71.7	9.52	103.4
6	185.8	13.96	154.5
7	95.3	19.80	219.2
8	192.5	23.34	269.3

Table 5.1
Nonlinear iteration

For $\lambda = 1$, the new sequence is equivalent to the old. Values of $\lambda > 1$ give overrelaxation, while $\lambda < 1$ results in underrelaxation. But while underrelaxation slows considerably the departure from the true solution seen in figures (5.2) and (5.3), even values of λ as small as 0.10 fail to produce convergence.

Strictly speaking, these results do not prove the divergence of the nonlinear algorithm. The solution of the linearized problem, on which it depends, involves errors which must be taken into account. It is possible that even when the exact solution ψ is used as a first guess, those errors push ψ_1 outside the radius of convergence on the first iteration. If this is in fact the cause of the divergence seen in figures (5.2) and (5.3), it implies that the radius of convergence must be quite limited. While errors introduced in solving the linearized problem might be reduced, they are already small enough to establish a very restrictive upper bound on ϵ. If convergence is possible at all, it will only be obtained with a first guess ψ_0 that differs from the true solution by an amount scarcely larger than uncertainties of measurement. So while these results do not establish the divergence of the nonlinear iteration in an absolute sense, it clearly must be ruled out as a practical method.

5.3. The Steady State Navier-Stokes Equations

Comparison with a related problem may throw some light on the failure of the nonlinear algorithm for the omega equation. The Navier-Stokes equations

$$\nabla^2 \zeta + R \left(\frac{\partial \psi}{\partial x} \frac{\partial \zeta}{\partial y} - \frac{\partial \psi}{\partial y} \frac{\partial \zeta}{\partial x} \right) = 0$$
$$\nabla^2 \psi = \zeta \tag{5.1}$$

(Greenspan, 1974) describe the steady state circulation of an viscous incompressible fluid in a square cavity. Boundary conditions

$$\psi = 0, \quad \frac{\partial \psi}{\partial n} = 0$$

establish that tangential and normal components of velocity vanish at the three (closed) sides of the cavity, while the conditions

$$\psi = 0, \quad \frac{\partial \psi}{\partial n} = -1$$

on the fourth (open) side corresponds to an external driving force. For small values of the Reynolds number R, viscous forces are dominant, while inertial forces become more important as R increases.

Kawaguti (1961) describes a finite difference method for solving the cavity flow problem, but that method is divergent for $R > 128$. Through the careful use of backward-forward difference approximations for the vorticity advection terms, and related expedients, Greenspan (1974) achieves convergence for Reynolds numbers as large as 10^5. Like the algorithm for the nonlinear omega equation described above, Greenspan's method is based on the repeated solution of a linearized problem. The technique depends for its success on the presence of the fourth order term $\nabla^2 \zeta$, which makes possible a diagonally dominant set of finite difference equations. (Though the practical problems of maintaining

diagonal dominance increase with increasing R .)

The parallels between this problem and the omega equation are clear. Equation (5.1) approaches equation (1.1) as $R \rightarrow \infty$. (The coriolis parameter f and the fact that equation 1.1 is not homogeneous are presumed to be of secondary importance.) The omega equation can be regarded as the limiting case of (5.1) for infinite Reynolds number, i.e. perfectly inviscid flow. Similarities between the two problems should probably not be exaggerated – the presence of a fourth order term in (5.1) represents a fundamental difference in character. But in view of the increasing difficulties of the cavity flow problem as R becomes large, the intractability of the omega equation should not come as a surprise.

5.4. Conclusions

In the preceding pages we have exhausted the obvious methods of attacking the nonlinear omega equation, or at least those that are obvious to this writer. (Another alternative is briefly discussed – and dismissed – in appendix B.) In fact, the methods presented here represent only a fraction of those that were actually tried. The weaknesses of many methods not mentioned are obvious only in retrospect.

It is customary to view the behavior of a differential equation as primarily determined by the highest order terms. Thus in linearizing a problem it is the

lower order terms that are generally held constant. Experience with the omega equation suggests that this approach requires some caution. It is now clear that the factors $\frac{\partial \psi}{\partial x}$ and $\frac{\partial \psi}{\partial y}$ in equation (1.1) have a steering function. Small changes in these first order terms can result in large displacements of values computed for higher order vorticity terms. The way to avoid this difficulty is not clear.

While the nonlinear problem remains intractable, solution of the linearized omega equation is a useful first step. That solution is sufficiently accurate to allow recovery of the 500 mb height field with errors of less than 10 meters. This result approaches the level of uncertainties in physical observation. Improved techniques for interpolation and numerical integration could reduce errors still further. Methods used to solve the linearized problem are directly applicable to first order equations with highly curved characteristics, where more traditional approaches are likely to result in instability.

Bibliography

Ahlberg, J. H., E. N. Nilson, and J. L. Walsh, *The Theory of Splines and Their Application,* Academic Press, New York, 1967.

Arnason, G., "A convergent method for solving the balance equation," *Journal of Meteorology*, vol. 15, pp. 220-225, 1957.

Birkhoff, Garrett, "Piecewise bicubic interpolation and approximation in polygons," in *Approximations With Special Emphasis on Spline Functions*, ed. I. J. Schoenberg, pp. 185-221, Academic Press, New York, 1969.

Bolin, B., "An improved barotropic model and some aspects of using the balance equation for three dimensional flow," *Tellus*, vol. 8, pp. 61-73, 1956.

Briggs, Ian C., "Machine contouring using minimum curvature," *Geophysics*, vol. 39, pp. 39-48, 1974.

Carrier, George F. and Carl E. Pearson, *Partial Differential Equations,* Academic Press, New York, 1976.

Clark, Leo C., "Hemispheric solution of the omega equation including terrain and surface frictional effects" (master's thesis in meteorology), U.S Naval Postgraduate School, Monterey, 1962.

Danard, Maurice, "Incorporating satellite cloud observations into 500 MB analysis and prediction", University of Victoria, Department of Computer Science, 1982.

Djuric, Dusan, "Note on the estimation of vertical motion by the omega equation," *Monthly Weather Review*, vol. 97, pp. 902-904, 1969.

Greenspan, Donald, "Numerical studies of prototype cavity flow problems," *Computer Journal*, vol. 12, pp. 88-93, 1969.

Greenspan, Donald, *Discrete Numerical Methods in Physics and Engineering,* Academic Press, New York, 1974.

Hadamard, Jacques, *Lectures on Cauchy's Problem,* Yale University Press, 1923.

Haltiner, George J., "Computation of the large scale vertical velocity," *Journal of Applied Meteorology*, vol. 2, pp. 242-259, 1963.

Haltiner, George J. and Roger Terry Williams, *Numerical Prediction and Dynamic Meteorology,* John Wiley and Sons, New York, 1980.

Hansen, John, "Vertical motion calculation and satellite cloud observations over the western and central U.S.," *Journal of Applied Meteorology*, vol. 4, pp. 18-30, 1965.

Holton, James R., *An Introduction to Dynamic Meteorology,* Academic Press, New York, 1972.

Ivanyan, G. A., "Calculating the vertical movement fields using satellite cloud data," *Meteorology and Hydrology* (English translation of *Meteorologia i Gidrologiya*), vol. 1, pp. 44-51, 1972.

Iverson, T. and T. E. Nordeng, "A convergent method for solving the balance equation," *Monthly Weather Review*, vol. 110, pp. 1347-1353, 1982.

Kawaguti, M., "Numerical solution of the Navier-Stokes equations for the flow in a two-dimensional cavity," *Journal of the Physical Society of Japan*, vol. 16, pp. 2307-2318, 1961.

Lancaster, P. and K. Salkauskas, *A Survey of Curve and Surface Fitting,* published by the authors, Calgary, [1977?].

Paegle and Tomlinson, "Solution of the balance equation by Fourier transform and Gauss elimination," *Monthly Weather Review*, vol. 103, pp. 528-535, 1974.

Penner, C. M., "An operational method for the determination of vertical velocities," *Journal of Applied Meteorology*, vol. 2, pp. 235-241, 1963.

Taylor, John D., P. Richards and R. Halstead, "Computer Routines for Surface Generation and Display" (Manuscript Report Series No. 16), Marine Science Branch, Department of Energy Mines and Resources, Ottawa, 1971.

APPENDIX A

Preliminary Computations

A.1. The Balance Equation

In solving the linearized balance equation

$$f\nabla^2\psi + \nabla f\cdot\nabla\psi = g\nabla^2 z \qquad \text{(A.1)}$$

for the stream function, an overrelation factor of 1.77 was found to give the most rapid convergence. Iteration continued until successive approximations to ψ agreed everywhere to a specified tolerance ψ_{tol}. Equation (A.1) was then solved a second time – this time in the opposite direction – in an attempt to recover the 500 millibar height z. The optimum relaxation factor for this problem was approximately 1.69, and various values of z_{tol} were used to terminate the iteration. Table (A.1) shows that the error $\max | z_1 - z_0 |$ in the recovered 500 millibar height is a function of both ψ_{tol} and z_{tol}. Even with $\psi_{tol} = 10^3\ m^2/sec$ it is possible to recover the original value of z with a maximum error of 3.4×10^{-3} meters. With the value $\psi_{tol} = 1.0\ m^2/sec$ that was used for the final computation of the stream function, that error is reduced to 4.3×10^{-5} meters.

tolerance for z (meters)	max $\mid z_1 - z_0 \mid$			
	tolerance for ψ (meters^2/sec)			
	10^3	10^2	10^1	10^0
10^{-2}	1.0×10^{-3}	3.5×10^{-4}		
10^{-4}	2.8×10^{-3}	1.5×10^{-3}	6.2×10^{-5}	
10^{-6}	3.4×10^{-3}	2.2×10^{-3}	4.6×10^{-4}	3.6×10^{-5}
10^{-8}	3.4×10^{-3}	2.2×10^{-3}	4.7×10^{-4}	4.3×10^{-5}
10^{-10}		2.2×10^{-3}	4.7×10^{-4}	4.3×10^{-5}
10^{-12}			4.7×10^{-4}	4.3×10^{-5}

Table A.1
Solving the linearized balance equation

A.2. Solving for Vertical Velocity

In solving equation (1.1) for ω, the most rapid convergence was obtained with a relaxation factor of 1.55. After 97 iterations, successive approximations differed by no more than 2.15×10^{-17} Pa/sec. No further improvement was possible with double precision machine arithmetic.

APPENDIX B

An Alternative Second Order System

Equation (3.1) shows one way that the omega equation can be written as a linked first and second order system. A less obvious alternative is based on the wind components

$$u = -\frac{\partial \psi}{\partial y} \qquad v = \frac{\partial \psi}{\partial x}$$

Since the rotational wind is non-divergent, we have

$$\frac{\partial u}{\partial x} + \frac{\partial v}{\partial y} = 0 \tag{B.1}$$

Differentiating with respect to x gives

$$\frac{\partial^2 v}{\partial x \, \partial y} = -\frac{\partial^2 u}{\partial x^2} \tag{B.2}$$

while differentiating with respect to y we have

$$\frac{\partial^2 u}{\partial x \, \partial y} = -\frac{\partial^2 v}{\partial y^2} \tag{B.3}$$

The vorticity ς is the vertical component of curl **V**:

$$\varsigma = \frac{\partial v}{\partial x} - \frac{\partial u}{\partial y}$$

Differentiating with respect to x:

$$\frac{\partial \varsigma}{\partial x} = \frac{\partial^2 v}{\partial x^2} - \frac{\partial^2 u}{\partial x \, \partial y}$$

And with respect to y:

$$\frac{\partial \varsigma}{\partial y} = \frac{\partial^2 v}{\partial x \, \partial y} - \frac{\partial^2 u}{\partial y^2}$$

Substituting for mixed second partial derivatives from (B.2) and (B.3) gives

$$\frac{\partial \varsigma}{\partial x} = \nabla^2 v \qquad \frac{\partial \varsigma}{\partial y} = -\nabla^2 u$$

These expressions can be substituted into (1.6), which then, along with equation (B.1) forms the system

$$u\,(-\nabla^2 v + \frac{\partial f}{\partial x}) + v\,(\nabla^2 u + \frac{\partial f}{\partial y}) = a\,\nabla^2 \omega + b\,\omega \tag{B.4}$$

$$\frac{\partial u}{\partial x} + \frac{\partial v}{\partial y} = 0 \tag{B.5}$$

This alternative is included here for completeness, but did not lead to any useful algorithm. If v is treated as a known function, (B.4) appears as a linear second order equation in u :

$$\nabla^2 u + p\,(x\,,y\,)u = q\,(x\,,y\,) \tag{B.6}$$

where

$$p = \frac{1}{v}\,(\nabla^2 v - \frac{\partial f}{\partial x})$$

and

$$q = \frac{1}{v}\,(a\,\nabla^2 \omega + b\,\omega) - \frac{\partial f}{\partial y}$$

Despite its resemblance to the Helmholtz equation, (B.6) proved remarkably

intractable. Although the equation is elliptic, it is impossible to maintain diagonal dominance of the finite difference representation without resort, at least locally, to an extremely fine grid.

It is possible to imagine an algorithm that involves alternately solving (B.4) for u and (B.5) for v (or vice versa), but even if the difficulties mentioned above could be overcome, the convergence of such a scheme seems doubtful.

VITA

Surname: JONES Given Names: WARREN KENNETH

Place of Birth: Minneapolis, Minnesota Date of Birth: October 5, 1950

Educational Institutions Attended, with Dates of Entering and Leaving:

Hamline University, St. Paul, Minnesota	1968 to 1969
University of Minnesota, Minneapolis	1970 to 1979
University of Victoria	1982 to 1984

Degrees, Diplomas, Etc., Awarded, with Dates and Names of Institutions:

B. Sc. 1979 University of Minnesota
(with high distinction)

Honors and Awards:

University of Victoria Fellowship, 1983–1984

University of Victoria Fellowship, 1982–1983

Hamline University Freshman Mathematics Award, 1969

Hamline University Presidential Scholarship, 1968–1969

Publications:

Jones, W. K. and T. R. Carroll, "Error Analysis of Airborne Gamma Radiation Soil Moisture Measurements", *Agricultural Meteorology*, **28**, 1983

Partial Copyright License

I hereby grant the right to lend my thesis (the title of which is shown below) to users of the University of Victoria Library, and to make *single copies only* for such users or in response to a request from the library of any other university, or similar institution, on its behalf or for one of its users. I further agree that permission for extensive copying of this thesis for scholarly purposes may be granted by me or a member of the University designated by me. It is understood that copying or publication of this thesis for financial gain shall not be allowed without my written permission.

Numeric Solution of the Non-Linear Omega Equation

Author

[redacted]

Warren Jones

August 30, 1985

Date